haematologica
Journal of the Ferrata Storti Foundation

Chromosomal rearrangement-enhanced mRNA stability drives the oncogenic potential of fusion genes in pediatric leukemia

by Xuejing Shao, Zhimei Xia, Minyi Cai, Chen Shao, Shaowei Bing, Tianrui Wang, Wenxin Du, Jiayi Liu, Diying Shen, Ji Cao, Bo Yang, Qiaojun He, Xiaojun Xu, Jingying Zhang and Meidan Ying

Received: May 19, 2025.
Accepted: November 6, 2025.

Citation: Xuejing Shao, Zhimei Xia, Minyi Cai, Chen Shao, Shaowei Bing, Tianrui Wang, Wenxin Du, Jiayi Liu, Diying Shen, Ji Cao, Bo Yang, Qiaojun He, Xiaojun Xu, Jingying Zhang and Meidan Ying. Chromosomal rearrangement-enhanced mRNA stability drives the oncogenic potential of fusion genes in pediatric leukemia.
Haematologica. 2025 Nov 13. doi: 10.3324/haematol.2025.288256 [Epub ahead of print]

Chromosomal rearrangement-enhanced mRNA stability drives the oncogenic potential of fusion genes in pediatric leukemia

Xuejing Shao[1, 2], Zhimei Xia[1], Minyi Cai[1], Chen Shao[1], Shaowei Bing[1], Tianrui Wang[1], Wenxin Du[1], Jiayi Liu[1], Diying Shen[3], Ji Cao[1], Bo Yang[1, 2, 4], Qiaojun He[1, 2, 5], Xiaojun Xu[3], Jingying Zhang[3, *], Meidan Ying[1,2,3,4,5*]

1, Institute of Pharmacology and Toxicology, Zhejiang Province Key Laboratory of Anti-Cancer Drug Research, College of Pharmaceutical Sciences, Zhejiang University, Hangzhou, 310058, China.

2, Nanhu Brain-computer Interface Institute, Hangzhou, 311100, China.

3, Division of Hematology-Oncology, the Children's Hospital Zhejiang University School of Medicine, Hangzhou, Zhejiang 310005, China.

4, School of Medicine, Hangzhou City University, Hangzhou, Zhejiang 310015, China.

5, Cancer Center, Zhejiang University, Hangzhou, 310058, China.

*****, **Corresponding authors:** Meidan Ying （mying@zju.edu.cn） and Jingying Zhang (zhangjy423@zju.edu.cn).

Declarations

Data-sharing statement

The datasets analyzed during the current study are available in the Therapeutically Applicable Research to Generate Effective Treatments (TARGET) portal (https://ocg.cancer.gov/programs/target). Raw data for RNA-sequencing are deposited at the NCBI GEO (GSE275289). For more additional data related to this subject, they are available from the corresponding author on reasonable request.

Funding

This work was supported by the Zhejiang Provincial Natural Science Foundation of China (No. LY24H080002 to JZ), the Natural Science Fund for Distinguished Young Scholars of Zhejiang Province (No. LR23H310001 to MY, No. LR24H310001 to XS), and the Fundamental Research Funds for the Central Universities (No. 226-2025-00136 to MY).

Competing interests

The authors declare no competing interests.

Authors' contributions

MY, XS and JZ conceived the study and analyzed data. MY and XS organized the figure and wrote the manuscript. JZ and DS collected the fusion and clinical information of our ALL cohort. XS, ZX and SB performed the fusion analysis. ZX, MC, CS, TW and WD performed the animal study and *in vitro* assay. XS, ZX, JL and XX performed and analyzed the RNA-sequencing data. JC, BY and QH conceived the experiments and helped organize the paper.

Abstract

Acute lymphoblastic leukemia (ALL), the most common type of pediatric leukemia, is frequently driven by fusion genes generated by chromosomal rearrangements. Compared with wild-type genes, many oncogenic fusions show increased expression and sustained functional activity that drives tumorigenesis. However, the mechanisms by which chromosomal rearrangements lead to functional enhancement remain largely elusive. In addition, although large-scale sequencing has identified numerous fusion events, the functional significance of most remains unclear. Here, we demonstrate that enhanced mRNA stability represents an important tumorigenic mechanism for oncogenic fusions, including classical PAX5 fusions. Based on this mechanism, we characterize a novel oncogenic fusion, STK38-PXT1, which exhibits upregulated STK38 mRNA levels and drives the development of ALL. Mechanistically, the increased mRNA stability results primarily from enhanced m6A modification of oncogenic fusions, which is attributable to “gene truncation” (as in PAX5 fusions) and “partner collaboration” (as in STK38-PXT1). Furthermore, the m6A reader IGF2BP3 is crucial for maintaining the high mRNA stability of oncogenic fusions. We further propose venetoclax as an innovative and clinically available therapy for ALL driven by these oncogenic fusions characterized by high mRNA stability. Our study not only highlights mRNA stabilization as a crucial mechanism by which oncogenic fusions to drive tumorigenesis, but also presents a promising therapeutic strategy for patients with ALL.

Key Words: Acute lymphoblastic leukemia; oncogenic fusion, mRNA stability; m6A modification; venetoclax

Introduction

Acute lymphoblastic leukemia (ALL) is the most common type of pediatric cancer that represents a hematologic malignancy comprising multiple subtypes[1,2]. Clinically, it is categorized into genetically distinct subgroups mainly based on chromosomal rearrangement-induced specific gene fusions, such as ETV6-RUNX1, PAX5 fusions, and so on[3]. Currently, chemotherapy is still used as the standard therapy, which poses significant long-term toxic risks such as cardiotoxicity[4]. While BCR-ABL1-targeted therapy exemplifies fusion-driven treatment success[5,6], most ALL fusions lack effective targeted strategies. Elucidating the mechanism by which chromosome rearrangements lead to abnormal function of wild-type genes will help to put forward new targeted strategies.

The current focus of fusion research primarily lies in individual studies of each fusion[7-10], leading to a lack of universality in research on carcinogenic mechanisms and intervention strategies. We ponder whether it is feasible to uncover a relatively universal oncogenic mechanism for fusions, which could potentially serve as a foundation for developing a generalized therapeutic strategy for intervening in different fusions. Meanwhile, although large-scale sequencing reveals many uncharacterized fusions in ALL[11], their clinical relevance remains unclear. It is urgent to rapidly identify oncogenic fusions from complex events. Thus, we also wonder if the identification of oncogenic fusions can be achieved based on this framework.

Protein function is precisely regulated at multiple levels, including transcription, post-transcriptional, translation, post-translational regulation. Compared to wild-type genes, various oncofusions exhibit continuously enhanced function to drive tumorigenesis. Several mechanisms have been suggested to account for the functional enhancement of oncogenic fusions. First, fusions such as P2RY8-CRLF2 can significantly activate transcription through promoter exchange, where the 5'UTR of P2RY8 triggers the obvious transcriptional upregulation of CRLF2[12]. Second, fusion proteins such as MLL-AF9 are more stable than wild-type proteins due to the loss of post-translational ubiquitination[13]. Third, kinase fusions such as ABL, ALK and RET fusions exhibit sustained kinase activation by dimerization[14]. However, the underlying mechanism by which chromosomal rearrangements lead to functional enhancement still remains largely elusive. So far, the regulatory mechanisms of

fusion proteins in post-transcriptional regulation, such as mRNA stability have not been reported.

The N6-methyladenosine (m6A) modification plays a pivotal role in modulating mRNA stability[15], abnormal alterations in m6A methylation and its modulators (writers, erasers and readers) have been reported to be closely associated with cancer[16,17]. However, it remains completely unknown whether m6A modification regulates the mRNA stability of fusions, thereby participating in the tumorigenicity of oncofusions. In addition, the molecular events such as mRNA degradation and stabilization that occur through m6A modification rely on m6A readers[18]. Among them, YTH domain-containing proteins generally destabilize m6A-containing mRNAs, whereas m6A-containing mRNA can be stabilized by other m6A reader proteins such as IGF2BPs[19,20]. Based on these, we suspect that the mRNA stability regulated by the m6A modification would be a potential critical oncogenic mechanism for fusions, and m6A readers especially those that can stabilize oncogenic fusions may hold promise as therapeutic targets in cancer.

In this study, we propose a model for the first time that chromosomal rearrangements enhance mRNA stability of fusions to drive leukemogenesis, and identify a novel oncogenic fusion STK38-PXT1. Mechanistically, mRNA stability of oncofusions including classical PAX5 fusions and the new STK38-PXT1 increases due to enhanced m6A modification, mainly driven by gene truncation and partner collaborations. Furthermore, we propose venetoclax as a promising drug for these oncofusion-driven ALL patients.

Methods

The fusion and gene expression of ALL samples

The fusion information and gene expression of 679 samples in TARGET ALL were supplied by the Therapeutically Applicable Research to Generate Effective Treatments (TARGET) portal (https://ocg.cancer.gov/programs/target). The fusion information and gene expression of 172 samples in our ALL cohort were obtained by Children's Hospital of Zhejiang University School of Medicine (CNpALL).

The mRNA expression analysis of partner genes in patients with fusions

Fusions were first separated into left (L) and right (C) partners. Then the $\log_2$(FC) and

$-\log_{10}$(P_val) values were calculated by the different expression level between patients with or without harboring certain fusion using R packages dplyr and tidyverse (code: https://github.com/bingshaowei/ALL).

Animal studies

4- to 6-week-old female nude mice were purchased from Ziyuan@, China. BaF3 cells were transduced with PMSCV, STK38(WT) or STK38-PXT1 lentivirus. Then, BaF3 cells (1×10^6 cells) were injected subcutaneously into nude mice. The tumor formation rate was recorded daily. Tumors were monitored for 150 days before PCR/Sanger sequencing validation. Female NSG mice (4–6-week-old) were purchased from Nanfang Model Animal Center (China). A total of 6×10^6 transduced BaF3 cells were injected via the tail vein into NSG mice. Peripheral blood was collected 45 days post-transplantation, and the percentage of mouse CD19-positive ($mCD19^+$) cells was analyzed by flow cytometry, and overall survival was recorded. For treatment studies, venetoclax (100 mg/kg) was administered once daily by oral gavage.

MERIP-qPCR experimental procedure

The target gene was transfected into HEK293T or BaF3, and mRNA was extracted for m6A-IP using an m6A-specific antibody. The IP mixture, containing magnetic beads, RNase inhibitor, mRNA, IP buffer, and antibody, was incubated at 4°C for 4 hours, washed, and eluted. The purified mRNA was then quantified by qPCR using primers listed in **Table S1**.

Drug screening of FDA-approved antitumor drugs in the BaF3 cells

PAX5-ETV6 and STK38-PXT1 BaF3 cells were treated with FDA-approved drugs at clinical concentrations for 72 h, with viability measured by CellTiter-Glo 2.0. (Promega, Beijing, China).

Statistical analysis and reproducibility

All the data are presented as the mean ±SD. The statistical significance of differences between groups was determined by unpaired two-tailed Student's t-test analysis, one-way ANOVA with Tukey’s tests or two-way ANOVA. $*P < 0.05$, $**P < 0.01$, $***P < 0.001$, $\#P < 0.05$, $\#\#P < 0.01$, $\#\#\#P < 0.001$, n.s. $P > 0.05$.

Ethical Approval

Written informed consents from patients and approval from the Institutional Research

Ethics Committee of the hospital were obtained before the use of these clinical materials for research purposes. The Animal Research Committee at Zhejiang University approved all animal studies and animal care was provided in accordance with the institutional guidelines. All methods were performed in accordance with the relevant guidelines and regulations, including the Declaration of Helsinki.

Additional methods are provided in the Supplementary Methods.

Results

1. Chromosome rearrangement-enhanced mRNA stability contributes to carcinogenic activity of classical oncofusion genes

We introduced two ALL RNA-seq datasets: the TARGET ALL database (679 high-risk B-ALL/ALAL samples) and our CNpALL cohort from China Children's Hospital (172 pediatric B-ALL patients) (**Fig. 1A**). We identified a total of 1318 fusions (29 classical and 1289 unknown fusions) in TARGET ALL and CNpALL (**Fig. 1B**). The frequency of classical fusions was different between the TARGET ALL database and our ALL cohort which may be due to differences in patient population coverage, as the TARGET ALL did not encompass the entire spectrum of ALL samples (**Fig. 1C**). The fusion characteristics of our ALL cohort are consistent with those of the reported primary ALL sample set[11]. Then we compared the mRNA levels of partner genes in oncofusion-carried samples with that in all samples to evaluate the potential role of mRNA regulation in fusions. As shown in **Fig. 1D**, among 29 classical fusions, the obvious mRNA level upregulation of partner gene was found in 25 classical fusions, including 8 fusions with both left and right partner genes upregulation (Cluster I), 3 fusions with only left partner genes upregulated (Cluster II), and 14 fusions with only right partner genes upregulated (Cluster III). Among them, the high expression of P2RY8 in P2RY8-IGH was reported by literature[21], and the high expression of CRLF2 in P2RY8-CRLF2 resulted from promoter exchange[12]. These results suggest that the mRNA upregulation may be an important regulator to the oncogenicity of gene fusions.

Next, we further analyzed the expression of genes L and R in patients without the corresponding fusion. Results showed that the upregulation of partner R in classical fusions was highly positively correlated with the L/R ratio (R^2=0.6705), whereas that of partner L was not (R^2=0.0545) (**Fig. 1E**). These results demonstrate that the mRNA upregulation of partner

R in classical fusions is primarily a consequence of promoter exchange, whereas the increased mRNA level of partner L may be attributed to alternative regulatory mechanisms. Numerous studies have highlighted the crucial role of mRNA stability in the regulation of gene mRNA levels[22]. Then we used actinomycin D to inhibit mRNA synthesis and detected the mRNA degradation rate of fusions. As shown in **Fig. 1F** and **S1A**, the mRNA half-life of PAX5-ETV6 was significantly longer than that of PAX5(WT) both in pro-B BaF3 and HEK293T cells. Similarly, another classical fusion in Cluster I (TCF3-PBX1), also exhibited a markedly longer mRNA half-life compared with TCF3(WT) (**Fig. 1G**). These results indicate that the enhanced mRNA stability may contribute to the increased partner L expression of classical fusions, thereby improving the carcinogenic activity of oncofusions.

2. A novel STK38-PXT1 oncofusion is identified in ALL based on mRNA upregulation

Besides classical oncogenic fusions, we also identified various functionally unknown fusions (**Fig. 1B**). It is worth noting that among patients with fusions, 67.37% and 43.02% of patients had unknown fusions in TARGET and CNpALL, which were mutually exclusive with classical oncogenic drivers. Then, we also calculated the fold change in mRNA levels of partner genes in unknown fusion-carrying samples compared to no corresponding fusion-carrying samples. As shown in **Fig. 2A** and **2B**, the results showed that among the 1318 fusion genes, left partner genes (partner L) of 131 fusions and right partner genes (partner R) of 168 fusions showed enhanced mRNA levels, whereas there is only 1 fusion with decreased mRNA levels of a partner gene. Among them, 43 fusions (Cluster I) showed both mRNA upregulation of left and right partner genes, 88 fusions (Cluster II) exhibited only enhanced mRNA levels of left partner genes, and 125 fusions (Cluster III) displayed only increased mRNA levels of right partner genes (**Fig. 2C** and **Table S2**).

Since chromosome rearrangement-enhanced mRNA stability may contribute to carcinogenic activity of fusions, we speculate that we can search for novel oncogenic fusions based on the phenomenon of increased mRNA stability. Based on the possibility that mRNA upregulation of partner L in fusions may result from mRNA stability regulation, we first analyzed the unknown fusions with increased mRNA levels of partner L. As shown in **Fig. 2D**, with the annotations about whether the fusion was detected in other databases, including

ChimerSeq, TCGA_StarF2019, Mitelman, ChimerKB, ChimerPub and so on, we listed the Top10 recurrent fusions. Notably, increased mRNA level of STK38 was found in ALL compared with normal BM, and it was further enhanced in patients with unknown fusion STK38-PXT1 (**Fig. 3A**). STK38 kinase, functions in the DNA damage repair, cell cycle and apoptosis, is reported to be closely associated with the development of tumors[23]. Moreover, we found the mRNA level of STK38 was highest in ALL among 17 cancer types (**Fig. 3B**). Thus, we wonder whether STK38-PXT1 could directly drive the occurrence of ALL due to the hyper-activation of STK38.

To verify this hypothesis, we first confirmed the presence of STK38-PXT1 fusion in the patient by RT-PCR analysis and Sanger sequencing (**Fig. 3C**). We then demonstrated that the mRNA half-life of STK38-PXT1 was significantly longer than that of STK38(WT) both in BaF3 and HEK293T cells (**Fig. 3D and S1B**). To further investigate the oncogenic transformation activity of STK38-PXT1 fusion, we subcutaneously injected BaF3 cells transduced with vector-PMSCV virus, STK38(WT) and STK38-PXT1. As shown in **Fig. S2A**, tumors were detected only in nude mice injected with STK38-PXT1-overexpressing BaF3 cells, while no tumor was observed in mice injected with STK38(WT) as well as PMSCV-transduced cells. Notably, we detected the presence of STK38-PXT1 fusion in transplanted tumors using RT-PCR analysis and Sanger sequencing (**Fig. S2B**). Furthermore, we performed a bone marrow transplantation model to further examine whether the STK38-PXT1 fusion can promote leukemogenesis. As shown in **Fig. 3E**, the proportion of $mCD19^+$ cells in peripheral blood was markedly higher in the STK38-PXT1 group compared with the PMSCV control group. Meanwhile, mice injecting STK38-PXT1-overexpressing BaF3 cells exhibited significantly shortened survival (**Fig. 3F**). Together, we firstly identify a novel fusion gene, STK38-PXT1, which may drive oncogenic transformation in ALL.

3. STK38-PXT1 fusion drivers leukemogenesis through β-catenin signaling activation

To study the carcinogenic process of STK38-PXT1, we first evaluated its effect on the proliferation and colony formation of ALL cell lines (NALM-6 and REH) as well as pro-B BaF3 cell line. Results showed that STK38-PXT1 obviously promoted the proliferation and colony formation capacity of NALM-6 and REH cells (**Fig. 4A-B and S3A-B**). Additionally,

STK38(WT) overexpression also promoted cell proliferation. Combined with *in vivo* carcinogenic transformation results, we suspect that STK38 kinase itself may play a tumor-promoting effect in ALL, and STK38-PXT1 fusion can directly drive the leukemogenesis.

Next, we performed the differential gene analyses in BaF3 cells transfected with PMSCV, STK38(WT) and STK38-PXT1. As shown in **Fig. 4C**, compared with PMSCV, STK38-PXT1 and STK38(WT) commonly upregulated 1321 genes and downregulated 1702 genes (Cluster II). STK38-PXT1 specifically upregulated 1855 and downregulated 1030 genes (Cluster III), while STK38(WT) specifically upregulated 1715 and downregulated 1207 genes (Cluster I). In Cluster II, we identified various proliferation-associated genes, which may account for the ability of both STK38 (WT) and STK38-PXT1 to promote cell proliferation in vitro (**Fig. 4D** Left). We also observed a large number of genes specifically upregulated only in STK38-PXT1 (Cluster III), which may be key drivers of the oncogenicity of STK38-PXT1 (**Fig. 4D** Right). Meanwhile, STK38-PXT1 obviously promoted the proliferation and clonogenesis capacity of BaF3 cells, while the kinase mutant STK38-PXT1(K118R) did not (**Fig. 4E and S4A-B**). Therefore, we analyzed the differential pathway of STK38-PXT1 and STK38(WT) as well as their K118R mutants. As displayed in **Fig. 4F**, the gene set variation analysis (GSVA) in hallmark pathways demonstrated that various cancer-related pathways were activated by STK38-PXT1, such as WNT_BETA_CATENIN_SIGNALING, NOTCH_ SIGNALING, and KRAS_ SIGNALING_UP, while STK38-PXT1(K118R) did not, indicating that the kinase activity of STK38 may be associated with the tumorigenic effects of the fusion. Furthermore, enrichment of WNT_BETA_CATENIN_SIGNALING were also observed in STK38-PXT1 fusion-carring leukemia samples compared with other ALL samples (**Fig. 4G**). Therefore, we suspected that STK38-PXT1 fusion might drive leukemogenesis by activating Wnt-β-catenin signaling.

Given that phosphorylation of GSK3β at Ser9 facilitates the transcriptional activation of β-catenin[24], we assessed the effect of STK38-PXT1 on GSK3β phosphorylation. Results showed that the level of p-GSK3β (Ser9) was markedly increased in STK38-PXT1-overexpressed cells compared to STK38-overexpressed cells (**Fig. S4C**), suggesting that the increased p-GSK3β (Ser9) might be contributed to the activation of

β-catenin signaling in the STK38-PXT1 positive ALL cells. To further investigate the potential mechanism, we performed proteomic analyses to characterize the binding proteins of STK38-PXT1 versus STK38 (WT). Results showed that STK38-PXT1 exhibited increased association with several proteins, with the top five being RPS18, GNB2L1, RPS25, HNRNPD and AGL (**Fig. S4D-E**). Among them, GNB2L1 (also known as RACK1) is reported to bind and stabilize PKC[25,26], which has been reported to promote GSK3β phosphorylation at Ser9[27]. Based on this, we hypothesize that enhanced interactions with proteins such as RACK1 may contribute to increased GSK3β (Ser9) phosphorylation and activation of β-catenin signaling during STK38-PXT1-induced leukemogenesis.

4. The mRNA stability upregulation of fusion is attributed to enhanced m6A modification due to gene truncation and partner collaboration.

To further investigate the molecular mechanism underlying the mRNA stability upregulation of fusions, we chose the classical fusion PAX5-ETV6 and the newly identified fusion STK38-PXT1 as the research subjects. Given that the generation of fusion involves two steps, gene truncation due to chromosomal breakage and partner collaboration due to aberrant chromosomal recombination (**Fig. 5A**), we first determined the mRNA level of partner genes in fusions containing left or right genes. For PAX5-ETV6, we analyzed the mRNA level in the different fusion genes with PAX5 or ETV6 from pan-cancer database (**Fig. S5A**). Results showed that similar to PAX5-ETV6, the expression of PAX5 gene was significantly upregulated in all other PAX5 fusions, whereas the level of ETV6 fusion partners was unchanged (**Fig. 5B**), indicating that the gene truncation may contribute to the increased mRNA level in PAX5 fusions Meanwhile, no significant change of STK38 expression was observed in other STK38 fusions, whereas the level of the PXT1 fusion partner was upregulated in different PXT1 fusions (**Fig. 5C** and **S5B**), suggesting the PXT1 partner may help enhance the mRNA level of partners such as STK38. To further investigate the role of gene truncation and partner collaboration in the increased mRNA stability of PAX5-ETV6 and STK38-PXT1 fusions, we introduced the PAX5(N) and STK38(N). As shown in **Fig. 5D** and **Fig. S5C**, the mRNA half-life of PAX5-ETV6 as well as PAX5(N) was significantly longer than that of PAX5(WT) both in BaF3 and HEK293T cells. For

STK38-PXT1, the mRNA half-life of STK38-PXT1 was significantly longer than that of STK38(WT), while that of STK38(N) was not (**Fig. 5E, Fig. S5D**). Collectively, these findings indicate that the gene truncation and partner collaboration may regulate the mRNA stability of PAX5 fusion and STK38-PXT1.

Given that m6A modification is an important way to modulate mRNA stability, thus we compared the m6A modification level of the fusion gene and the truncated gene by Methylated RNA Immunoprecipitation (MeRIP) assay (**Fig. S5E**). Results showed that the m6A modification level of PAX5-ETV6 and PAX5(N) was higher than that of PAX5(WT) in BaF3 and HEK293T cells (**Fig. 6A, Fig. S5F**). Meanwhile, the m6A modification level of STK38-PXT1 was higher than that of STK38(WT) and STK38(N) (**Fig. 6B, Fig. S5G**). These results were highly consistent with the mRNA stability changes observed in PAX5-ETV6 and STK38-PXT1. Then, we further analyzed the potential m6A modification sites within PAX5-ETV6 and STK38-PXT1. We first used the m6A prediction tool SRAMP to identify putative methylation sites within both PAX5-ETV6 and STK38-PXT1 fusion, and then we generated point mutant constructs at predicted adenines to find the potential m6A sites. For PAX5-ETV6, predicted potential methylation sites were A43 and A48 in the PAX5 segment and A614, A843, A1322 and A1437 in the ETV6 segment (**Table S3**). Given the comparable m6A levels between PAX5(WT) and PAX5(N), we hypothesized that the functional m6A sites may be located on the PAX5 segment. mRNA stability assays and MeRIP-qPCR assay results showed that the A48T mutation markedly reduced the half-life and m6A enrichment of PAX5 transcript, whereas the A43T mutation had no significant effect (**Fig. 6C-D**). For STK38-PXT1, predicted m6A sites were located exclusively within the STK38 segment (A545, A565, A602, A662, A681, A689, A708 and A727) (**Table S4**). Based on SRAMP scores, we selected the top two sites to evaluate. Results showed that both A727T and A708T mutations significantly reduced mRNA stability and m6A modification of STK38-PXT1 compared with the wild-type STK38 (**Fig. 6E-F**). Taken together, these results suggest that enhanced m6A modification due to gene truncation and partner collaboration may contribute to the enhanced mRNA stability of fusions.

5. m6A reader IGF2BP3 is responsible for maintaining the high stability of fusion

mRNA.

The m6A modification level is regulated by m6A methyltransferases (Writers) and demethylases (Erasers), and its regulation of mRNA stability requires reader proteins[16]. We suspect that key m6A readers stabilizing oncofusions could be promising therapeutic targets. Thus, we first analyzed the expression of m6A modulators (writers, erasers and readers) in ALL samples carrying PAX5 fusion and STK38-PXT1 fusion. Interestingly, the m6A reader IGF2BP3 was specifically upregulated in both PAX5 fusion and STK38-PXT1 fusion samples (**Fig. 7A-B** and **Fig. S6A**). And compared with other classical oncofusions, patients carrying PAX5 fusions showed the highest level of IGF2BP3 (**Fig. 7C**). In addition, the IGF2BP3 upregulation in KMT2A fusions is consistent with the literature[28]. Furthermore, shIGF2BP3 reduced mRNA stability of PAX5(N) and PAX5-ETV6 but not PAX5(WT) (**Fig. 7D**), and the mRNA half-life of STK38-PXT1 rather than STK38(WT) and STK38(N) was markedly shortened by shIGF2BP3 (**Fig. 7E**). These results indicate that IGF2BP3 may be the crucial reader to regulate the high mRNA stability of these fusions.

Next, to identify the potential therapeutic effect of IGF2BP3 in ALL driven by fusions with high mRNA stability, we investigated the effect of silencing IGF2BP3 in the proliferation of PAX5-ETV6 and STK38-PXT1 overexpressing BaF3 cells. As shown in **Fig. 7F-G**, we found that compared with PAX5(WT), shIgf2bp3 (#1 and #2) had a stronger inhibitory effect on cell proliferation on PAX5-ETV6 as well as PAX5(N). Similar to PAX5-ETV6, the inhibition rate of shIgf2bp3 in the STK38-PXT1 overexpressing BaF3 cells was higher than that in STK38(WT) overexpressing BaF3 cells, while this enhanced inhibitory effect was not observed in STK38(WT) overexpressing BaF3 cells (**Fig. 7H**). These results suggest IGF2BP3 as a novel candidate for therapeutic intervention for ALL patients driven by these fusions with stabilized mRNA.

Given that IGF2BP3 was elevated in PAX5 fusion and STK38-PXT1-positive ALL (**Fig. S6A**), we assessed whether other IGF2BP3 target genes were upregulated. Although IGF2BP3 can stabilize *c-MYC* in KMT2A-rearranged ALL[29], c-MYC was not increased in our fusion-positive cells (**Fig. S6B**). Comparing upregulated genes in these patients with IGF2BP3 RIP-seq data revealed 125 overlapping candidates, including various cancer-related genes (**Fig. S6C-D**), which may represent potential IGF2BP3 targets in this subset of ALL.

Meanwhile, we also explored potential mechanisms underlying IGF2BP3 upregulation in these patients. We found that BRD4, a reported transcriptional activator of IGF2BP3[30], was significantly elevated in both fusion-positive subtypes (**Fig. S6E**) and in IGF2BP3-high versus IGF2BP3-low ALL samples (**Fig. S6F**), suggesting that BRD4 upregulation may contribute to IGF2BP3 overexpression in this context.

6. Venetoclax specifically inhibits mRNA high-stability fusion-driven ALL

Based on the above finding that shIGF2BP3 could effectively inhibit the cell proliferation-promoting ability of PAX5-ETV6 and STK38-PXT1, targeting IGF2BP3 may be the ideal strategy for these fusion-driven ALL. Due to the lack of approved IGF2BP3 inhibitors, we next sought to search for potential clinically accessible marketed drugs with potential efficacy against PAX5-ETV6- or STK38-PXT1-rearranged ALL. First, we evaluated the inhibition rate of 102 FDA-approved antitumor drugs in the BaF3 cells that overexpressed PAX5-ETV6 and STK38-PXT1. Results showed that the inhibition rate of venetoclax in the PAX5-ETV6 group was 30.63% higher than that in the PAX5(WT) group, ranking the second among 102 antitumor drugs (**Fig. 8A**). For STK38-PXT1, the inhibition rate of venetoclax in the STK38-PXT1 cells was 48.78% higher than that in the STK38(WT) group, ranking first among 102 anti-tumor drugs (**Fig. 8B**). Additionally, we also analyzed the drug-response profiles according to IGF2BP3 expression levels in ALL cells, and found that venetoclax cytotoxicity was significantly greater in IGF2BP3-high cells (**Fig. 8C** and **S7A-B**). Thus, we hypothesized that venetoclax may represent a potential therapeutic agent for PAX5-ETV6- or STK38-PXT1-positive ALL.

Furthermore, we assessed the apoptosis-inducing effect of venetoclax in PAX5-ETV6 and STK38-PXT1 overexpressing cells. Results showed that compared with vector-PMSCV (22.54 ± 1.30%) and PAX5(WT) (28.37 ± 7.52%), the apoptosis rate of PAX5-ETV6 cells upon to venetoclax was further enhanced (70.85 ± 3.45%) (**Fig. 8D** and **S7C**). Similarly, a higher apoptosis rate induced by venetoclax was observed in STK38-PXT1 cells (57.34 ± 3.58%) than STK38(WT) (28.79 ± 2.98%) and vector-PMSCV (15.71 ± 0.59%) cells (**Fig. 8E** and **S7D**). Consistently, dose-dependent apoptosis induction by venetoclax was observed in both PAX5-ETV6 and STK38-PXT1 overexpressing cells (**Fig. S7E**). These results indicate

that venetoclax exhibited a selective cellular activity-inhibitory and apoptosis-inducing effect on BaF3 cells carrying PAX5-ETV6 and STK38-PXT1.

To explore the underlying mechanism, we first assessed the expression of BCL2 in BaF3 cells stably expressing either PAX5-ETV6 or STK38-PXT1 fusion genes. Results showed that the expression of BCL2 as well as other apoptotic players in cases carrying PAX5 fusions or STK38-PXT1 was comparable to that in the remaining patients (**Fig. S8A-B**). Then, we performed gene set enrichment analysis (GSEA) comparing PAX5 fusion and STK38-PXT1 fusion positive versus fusion-negative cases. We found that the OXIDATIVE_PHOSPHORYLATION (OXPHOS) pathway was significantly downregulated in both PAX5-ETV6 and STK38-PXT1 positive samples (**Fig. 8F-G**). This is noteworthy as previous studies have shown that reduced OXPHOS activity is strongly associated with heightened venetoclax sensitivity in AML[31-34]. Taken together, we hypothesize that decreased OXPHOS activity is a key vulnerability that contributes to the enhanced venetoclax sensitivity observed in PAX5-ETV6 or STK38-PXT1 expressing cells.

Finally, we evaluated the anti-leukemic activity of venetoclax *in vivo* using NSG mouse xenograft models established by intravenous engraftment of BaF3 cells expressing PAX5-ETV6 or STK38-PXT1. Results showed that venetoclax significantly suppressed the expansion of circulating $mCD19^{+}$ cells in both two leukemia models (**Fig. 8H**) and significantly prolonged the overall survival of leukemic mice (**Fig. 8I**), confirming its potent *in vivo* efficacy. Collectively, these results demonstrate that venetoclax exerts potent and selective anti-leukemic activity against PAX5-ETV6 and STK38-PXT1-driven ALL.

Discussion

Emerging evidence suggests that m6A methylation plays a critical role in cancer through various mechanisms. Alterations in m6A modification of various tumor-promoting genes like BRD4, MYC, SOCS2 and EGFR are important in cancer pathogenesis and progression[18]. Here, we first report that the m6A modification alteration is important for oncogenic fusions. Both the well-established oncogenic fusion PAX5-ETV6 and the novel oncofusion STK38-PXT1 show upregulated mRNA stability compared with wild-type PAX5 and STK38. Interestingly, we find that the increased mRNA stability separately results from “gene truncation” and “partner collaboration”. It is reported that exon architecture controls mRNA

m6A suppression through Exon Junction Complexes (EJCs)[35]. It is possible that gene truncation may lead to the loss of interaction between EJCs and mRNA, followed by the m6A modification up-regulation. For STK38-PXT1, inclusion of PXT1 may rewire the protein-protein interaction landscape, which may be associated with increased stability of the STK38 mRNA. Future work is needed to define how PAX5 C-terminal truncation and the PXT1 partner promote m6A modification of these fusions.

While gene fusion events in cancers have been extensively documented, their oncogenic functions remain largely unknown[36]. Currently, the approaches to identify key oncogenic fusions are mainly based on clinical information and unique transcriptional characteristics. For example, we have previously identified a novel gene fusion RUNX1-ZNF423 in a 1-year-old male AML patient with repeated relapse and chemoresistance[37]. St. Jude Children's Research Hospital illustrated new oncogenic subtype with DUX4 fusion that marked by a unique paradigm of transcription factor deregulation in leukemia[38]. A study about the transcriptional landscape of B-ALL based on an international study of 1,223 cases identified new ZNF362 fusion[39]. Here, combined with enhanced mRNA levels and mutual exclusivity with classical oncogenic drivers, we discover a novel oncogenic fusion STK38-PXT1. In addition, we also identified 256 fusions such as TRDV2-TRAC, FBRSL1-NOC4L and others with enhanced partner mRNA levels, whose function needs further investigation.

STK38 is composed of 13 exons, with exons 1-3 encoding the N-terminal regulatory (NTR) domain and exons 3-11 encoding the kinase domain[40]. The STK38-PXT1 fusion protein retains all N-terminal regulatory domains and portions of the kinase domain (exons 3-8). Our RNA-seq analysis indicates that activation of the β-catenin pathway may contribute to the oncogenic mechanism of STK38-PXT1. Moreover, combined the proteomic data, we hypothesize that enhanced interactions between STK38-PXT1 and proteins such as RACK1 may contribute to increased GSK3β phosphorylation at Ser9 and the activation of β-catenin signaling during leukemogenesis. Certainly, these interactions and their relationship to β-catenin activation needs further in-depth investigation.

Abnormal alterations in m6A modification have been reported to be closely associated with leukemia especially acute myeloid leukemia (AML). Multiple m6A modulators, such as writers METTL16[41], erasers FTO [42,43] and ALKBH5[44,45], readers YTHDF1[46], YTHDC1[47],

IGF2BP2[48] and IGF2BP3[49], are reported to regulate AML progression. Our study showed that IGF2BP3 may be the ideal target for PAX5-ETV6 or STK38-PXT1 fusion-driven ALL. Therefore, pharmacologic inhibition of IGF2BP3, for example with the small-molecule inhibitor AE-848, may represent a promising treatment strategy[50]. Furthermore, we showed that these fusion-positive ALL cells exhibit sensitivity to venetoclax. We found a marked suppression of OXPHOS in fusion-positive cases rather than BCL2 upregulation. It has been reported that low OXPHOS activity strongly correlates with heightened venetoclax sensitivity in leukemia[31-34]. Mechanistically, leukemic cells with intrinsically low OXPHOS rely heavily on BCL-2 to maintain mitochondrial outer membrane integrity; inhibition of BCL-2 in such cells rapidly triggers mitochondrial outer membrane permeabilization, cytochrome-c release, caspase activation, and prompt apoptosis[31]. Collectively, these findings suggest that reduced OXPHOS activity represents a metabolic vulnerability that underlies the increased venetoclax sensitivity of PAX5-ETV6 or STK38-PXT1 expressing cells.

Collectively, our findings unveil novel oncogenic mechanisms underpinned by m6A modification and mRNA stability in fusion genes. These insights not only facilitate the discovery of a novel oncogenic fusion, but also pave the way for innovative strategies aimed at unraveling oncogenic fusion events.

Abbreviations

ALL: Acute lymphoblastic leukemia; m6A: N6-methyladenosine; TARGET: Therapeutically Applicable Research to Generate Effective Treatments

Reference

1. Lilljebjorn H, Fioretos T. New oncogenic subtypes in pediatric B-cell precursor acute lymphoblastic leukemia. Blood. 2017;130(12):1395-1401.
2. Malard F, Mohty M. Acute lymphoblastic leukaemia. Lancet. 2020;395(10230):1146-1162.
3. Gokbuget N, Boissel N, Chiaretti S, et al. Diagnosis, prognostic factors, and assessment of ALL in adults: 2024 ELN recommendations from a European expert panel. Blood. 2024;143(19):1891-1902.
4. Inaba H, Mullighan CG. Pediatric acute lymphoblastic leukemia. Haematologica. 2020;105(11):2524-2539.
5. Mertens F, Johansson B, Fioretos T, Mitelman F. The emerging complexity of gene fusions in cancer. Nat Rev Cancer. 2015;15(6):371-381.
6. Ren R. Mechanisms of BCR-ABL in the pathogenesis of chronic myelogenous leukaemia. Nat Rev Cancer. 2005;5(3):172-183.
7. Olsen SN, Godfrey L, Healy JP, et al. MLL::AF9 degradation induces rapid changes in transcriptional elongation and subsequent loss of an active chromatin landscape. Mol Cell. 2022;82(6):1140-1155.e11.
8. Guo M, Chan THM, Zhou Q, et al. Core-binding factor fusion downregulation of ADAR2 RNA editing contributes to AML leukemogenesis. Blood. 2023;141(25):3078-3090.
9. Day RB, Hickman JA, Xu Z, et al. Proteogenomic analysis reveals cytoplasmic sequestration of RUNX1 by the acute myeloid leukemia-initiating CBFB::MYH11 oncofusion protein. J Clin Invest. 2023;134(4):e176311.
10. Heikamp EB, Henrich JA, Perner F, et al. The menin-MLL1 interaction is a molecular dependency in NUP98-rearranged AML. Blood. 2022;139(6):894-906.
11. Lilljebjorn H, Henningsson R, Hyrenius-Wittsten A, et al. Identification of ETV6-RUNX1-like and DUX4-rearranged subtypes in paediatric B-cell precursor acute lymphoblastic leukaemia. Nat Commun. 2016;7:11790.
12. Mullighan CG, Collins-Underwood JR, Phillips LA, et al. Rearrangement of CRLF2 in B-progenitor- and Down syndrome-associated acute lymphoblastic leukemia. Nat Genet. 2009;41(11):1243-1246.
13. Liu J, Tokheim C, Lee JD, et al. Genetic fusions favor tumorigenesis through degron loss in oncogenes. Nat Commun. 2021;12(1):6704.
14. Stransky N, Cerami E, Schalm S, Kim JL, Lengauer C. The landscape of kinase fusions in cancer. Nat Commun. 2014;5:4846.
15. Fu Y, Dominissini D, Rechavi G, He C. Gene expression regulation mediated through reversible m(6)A RNA methylation. Nat Rev Genet. 2014;15(5):293-306.
16. Wang T, Kong S, Tao M, Ju S. The potential role of RNA N6-methyladenosine in Cancer progression. Mol Cancer. 2020;19(1):88.
17. Wang Y, Wang Y, Patel H, et al. Epigenetic modification of m(6)A regulator proteins in cancer. Mol Cancer. 2023;22(1):102.
18. Jiang X, Liu B, Nie Z, et al. The role of m6A modification in the biological functions and diseases. Signal Transduct Target Ther. 2021;6(1):74.
19. Fang Z, Mei W, Qu C, et al. Role of m6A writers, erasers and readers in cancer. Exp Hematol Oncol. 2022;11(1):45.
20. Zaccara S, Ries RJ, Jaffrey SR. Reading, writing and erasing mRNA methylation. Nat Rev

Mol Cell Biol. 2019;20(10):608-624.

21. Fang Y, Wang M, Hu S, et al. Recurrent Novel P2RY8/IGH Translocations in B-Lymphoblastic Leukemia/Lymphoma. Front Oncol. 2022;12:896858.
22. Boo SH, Kim YK. The emerging role of RNA modifications in the regulation of mRNA stability. Exp Mol Med. 2020;52(3):400-408.
23. Qin B, Yu J, Nowsheen S, Zhao F, Wang L, Lou Z. STK38 promotes ATM activation by acting as a reader of histone H4 ufmylation. Sci Adv. 2020;6(23):eaax8214.
24. Song S, Mazurek N, Liu C, et al. Galectin-3 mediates nuclear β-catenin accumulation and Wnt signaling in human colon cancer cells by regulation of glycogen synthase kinase-3β activity. Cancer Res. 2009;69(4):1343-1349.
25. Besson A, Wilson TL, Yong VW. The Anchoring Protein RACK1 Links Protein Kinase Cε to Integrin β Chains: REQUIREMENT FOR ADHESION AND MOTILITY. J Biol Chem. 2002;277(24):22073-22084.
26. Rigas AC, Ozanne DM, Neal DE, Robson CN. The scaffolding protein RACK1 interacts with androgen receptor and promotes cross-talk through a protein kinase C signaling pathway. J Biol Chem. 2003;278(46):46087-46093.
27. Neary JT, Kang Y. P2 purinergic receptors signal to glycogen synthase kinase□3β in astrocytes. J Neurosci Res. 2006;84(3):515-524.
28. Tran TM, Philipp J, Bassi JS, et al. The RNA-binding protein IGF2BP3 is critical for MLL-AF4-mediated leukemogenesis. Leukemia. 2022;36(1):68-79.
29. Palanichamy JK, Tran TM, Howard JM, et al. RNA-binding protein IGF2BP3 targeting of oncogenic transcripts promotes hematopoietic progenitor proliferation. J Clin Invest. 2016;126(4):1495-1511.
30. Yang Y, Gao J, Shi H, et al. IGF2BP3 As a Prognostic Biomarker and Regulator of Metastasis in Merkel Cell Carcinoma. JID Innov. 2025;5(3):100355.
31. Lagadinou ED, Sach A, Callahan K, et al. BCL-2 inhibition targets oxidative phosphorylation and selectively eradicates quiescent human leukemia stem cells. Cell Stem Cell. 2013;12(3):329-341.
32. Chan SM, Thomas D, Corces-Zimmerman MR, et al. Isocitrate dehydrogenase 1 and 2 mutations induce BCL-2 dependence in acute myeloid leukemia. Nat Med. 2015;21(2):178-184.
33. Pollyea DA, Stevens BM, Jones CL, et al. Venetoclax with azacitidine disrupts energy metabolism and targets leukemia stem cells in patients with acute myeloid leukemia. Nat Med. 2018;24(12):1859-1866.
34. Stevens BM, Jones CL, Pollyea DA, et al. Fatty acid metabolism underlies venetoclax resistance in acute myeloid leukemia stem cells. Nat Cancer. 2020;1(12):1176-1187.
35. He PC, Wei J, Dou X, et al. Exon architecture controls mRNA m(6)A suppression and gene expression. Science. 2023;379(6633):677-682.
36. Hu X, Wang Q, Tang M, et al. TumorFusions: an integrative resource for cancer-associated transcript fusions. Nucleic Acids Res. 2018;46(D1):D1144-D1149.
37. Du W, Xia Z, Luo Z, et al. A novel gene fusion RUNX1/ZNF423 promotes leukemic relapse of NUP98-rearranged AML. Leukemia. 2023;37(11):2286-2291.
38. Zhang J, McCastlain K, Yoshihara H, et al. Deregulation of DUX4 and ERG in acute lymphoblastic leukemia. Nat Genet. 2016;48(12):1481-1489.

39. Li JF, Dai YT, Lilljebjorn H, et al. Transcriptional landscape of B cell precursor acute lymphoblastic leukemia based on an international study of 1,223 cases. Proc Natl Acad Sci U S A. 2018;115(50):E11711-E11720.
40. Martin AP, Aushev VN, Zalcman G, Camonis JH. The STK38-XPO1 axis, a new actor in physiology and cancer. Cell Mol Life Sci. 2021;78(5):1943-1955.
41. Han L, Dong L, Leung K, et al. METTL16 drives leukemogenesis and leukemia stem cell self-renewal by reprogramming BCAA metabolism. Cell Stem Cell. 2023;30(1):52-68.e13.
42. Li Z, Weng H, Su R, et al. FTO Plays an Oncogenic Role in Acute Myeloid Leukemia as a N(6)-Methyladenosine RNA Demethylase. Cancer Cell. 2017;31(1):127-141.
43. Huang Y, Su R, Sheng Y, et al. Small-Molecule Targeting of Oncogenic FTO Demethylase in Acute Myeloid Leukemia. Cancer Cell. 2019;35(4):677-691.e610.
44. Wang J, Li Y, Wang P, et al. Leukemogenic Chromatin Alterations Promote AML Leukemia Stem Cells via a KDM4C-ALKBH5-AXL Signaling Axis. Cell Stem Cell. 2020;27(1):81-97.e88.
45. Shen C, Sheng Y, Zhu AC, et al. RNA Demethylase ALKBH5 Selectively Promotes Tumorigenesis and Cancer Stem Cell Self-Renewal in Acute Myeloid Leukemia. Cell Stem Cell. 2020;27(1):64-80.e69.
46. Hong YG, Yang Z, Chen Y, et al. The RNA m6A Reader YTHDF1 Is Required for Acute Myeloid Leukemia Progression. Cancer Res. 2023;83(6):845-860.
47. Sheng Y, Wei J, Yu F, et al. A critical role of nuclear m6A reader YTHDC1 in leukemogenesis by regulating MCM complex-mediated DNA replication. Blood. 2021;138(26):2838-2852.
48. Weng H, Huang F, Yu Z, et al. The m(6)A reader IGF2BP2 regulates glutamine metabolism and represents a therapeutic target in acute myeloid leukemia. Cancer Cell. 2022;40(12):1566-1582.e1510.
49. Zhang N, Shen Y, Li H, et al. The m6A reader IGF2BP3 promotes acute myeloid leukemia progression by enhancing RCC2 stability. Exp Mol Med. 2022;54(2):194-205.
50. Shu C, Gu M-H, Zeng C, et al. Small-molecule exhibits anti-tumor activity by targeting the RNA m6A reader IGF2BP3 in ovarian cancer. Am J Cancer Res. 2023;13(10):4888.

Figure Legends

Figure 1 Chromosome rearrangement-enhanced mRNA stability contributes to carcinogenic activity of classical oncofusion genes. (**A**) Schematic diagram of the sample information, fusion identification and analysis process. (**B**) The fusion information in the TARGET ALL database and the CNpALL cohort. The detailed fusion genes in 679 ALL samples were downloaded from the Therapeutically Applicable Research to Generate Effective Treatments (TARGET) database. The 172 primary samples originated from the clinical pediatric leukemia sample cohort at the Children's Hospital of Zhejiang University School of Medicine (CNpALL). The fusion genes in samples were identified by STAR-Fusion based on the whole-transcriptome sequencing. (**C**) Difference in the frequency of classical oncofusions between the TARGET ALL database and our Chinese CNpALL cohort. (**D**) The mRNA expression of partner genes (Partner L and R) in patients with classical fusions and without the corresponding oncofusion. Red: Cluster I, fusions with both mRNA upregulation of left and right partner genes; Yellow: Cluster II, fusions with only enhanced mRNA levels of left partner genes; Blue: Cluster III, fusions with only increased mRNA levels of right partner genes; Gray: Cluster IV, fusions without increased mRNA level of left or right partner genes. (**E**) The correlation analysis between partner mRNA upregulation in fusions and the expression of wild-type gene. The fold change (FC) (fusion/no fusion) was calculated by comparing the mRNA level of partner gene in samples with fusion and that in other samples. The FC(Gene L/R) was calculated by comparing the mRNA levels of the partner genes in samples without fusions. (**F**) The mRNA half-life of PAX5(WT) and PAX5-ETV6. Genes were overexpressed in BaF3 cells, and mRNA synthesis was inhibited with actinomycin D (5 μg/mL). Samples were collected to extract mRNA at the indicated times after treatment with actinomycin. $t_{1/2}$ was calculated by simple linear regression. (**G**) The mRNA half-life of TCF3(WT) and TCF3-PBX1. (F-G) Data are represented as mean ± SD (n=3). The significance analysis was conducted by two-way ANOVA analysis. *, $P<0.05$, **, $P<0.01$ *vs.* indicated.

Figure 2 The prediction of potential oncofusions based on increased mRNA level

of left partner genes. (**A**-**B**) mRNA level analysis of partner genes in ALL with classical and unknown fusions. The fold change (FC) was calculated by comparing the mRNA level of partner genes in samples with fusions and that in other samples without corresponding fusion. P_val was calculated by two-tailed unpaired Student's t-test between samples with fusions and all samples. (A) The mRNA expression of left partner genes in patients with fusions. (B) The mRNA expression of right partner genes in patients with fusions. (**C**) The 256 fusions with significant mRNA regulation of partner genes. Red: Cluster I, fusions with both mRNA upregulation of left and right partner genes; Yellow: Cluster II, fusions with only enhanced mRNA levels of left partner genes, Blue: Cluster III, fusions with only increased mRNA levels of right partner genes. (**D**) The Top 10 recurrent unknown fusions with increased mRNA level of left partner genes. The recurrent fusions were identified through database comparison, including ChimerSeq, TCGA_StarF2019, Mitelman, ChimerKB, ChimerDB_PubMed, ChimerPub and other databases.

Figure 3 A novel STK38-PXT1 oncofusion is identified in ALL based on mRNA upregulation. (**A**) The mRNA expression levels of the STK38 gene in three different sample groups. Normal BM: healthy bone marrow samples collected by ourselves; Other ALL: ALL samples without STK38-PXT1 in our CNpALL cohort; STK38-PXT1: 4 samples specifically carrying the STK38-PXT1 fusion in our CNpALL cohort. (**B**) The mRNA expression levels of the STK38 gene in different types of cancer cell lines from the CCLE database. (**C**) Schematic diagrams of wild-type STK38 protein, wild-type PXT1 protein, and STK38-PXT1 fusion protein. (**D**) The mRNA half-life of STK38(WT) and STK38-PXT1 in BaF3 cells. Data are represented as mean ± SD (n=3). (**E**) Percentage of $mCD19^{+}$ cells in peripheral blood of NSG mice 45 days after intravenous transplantation of BaF3 cells transduced with PMSCV control or STK38-PXT1 lentivirus (n=5). **(F)** Kaplan-Meier overall survival curves of NSG mice transplanted with BaF3 cells expressing PMSCV control or STK38-PXT1(n=5). (A, D, E, F) The significance analysis was conducted using one-way ANOVA, two-way ANOVA, unpaired Student's *t*-test, or log-rank test, *, $P<0.05$; **, $P<0.01$; ***, $P<0.001$ *vs.* indicated.

Figure 4 STK38-PXT1 fusion drives leukemogenesis through β-catenin signaling activation. (**A**) Proliferation curve of NALM-6 cells overexpressing STK38-PXT1 and STK38(WT). (**B**) The clony formation ability of NALM-6 cells overexpressing STK38(WT), STK38-PXT1. (**C-D**) Venn diagram and heatmap of differential gene analysis between STK38-PXT1 and STK38(WT). The differential gene analysis was performed by comparing the gene expression profiles in BaF3 cells transfected with STK38-PXT1 and vector-PMSCV, or BaF3 cells transfected with STK38(WT) and vector-PMSCV. (C) The Venn diagram of differential gene analysis was shown between STK38-PXT1 and STK38(WT). Cluster I: only changed in STK38(WT); Cluster II: both changed in STK38(WT) and STK38-PXT1; Cluster III: only changed in STK38-PXT1. (D) Genes from Clusters II (Left) and III (Right). genes related to cell proliferation in Cluster II were indicated in the heatmap. (**E**) Proliferation curve of BaF3 cells overexpressing STK38-PXT1. BaF3 cells were transfected with lentivirus PMSCV, STK38(WT), STK38(K118R), STK38-PXT1, and STK38-PXT1(K118R). (**F**) Gene Set Variation Analysis (GSVA) Hallmark enrichment across PMSCV, STK38(WT), STK38(K118R), STK38-PXT1, and STK38-PXT1(K118R). (**G**) Left: Gene Set Enrichment Analysis (GSEA) Hallmark enrichment between samples with STK38-PXT1 and other ALL samples in our CNpALL cohort. Right: GSEA plots depicting enrichment of Wnt-β-catenin signaling in the transcriptional profiling of samples with STK38-PXT1 and other ALL samples in our ALL cohort. (A, B, E) Data are represented as mean ± SD (n=3). The significance analysis was conducted using one-way or two-way ANOVA analysis. n.s., $P>0.05$; *, $P<0.05$; ***, $P<0.001$ *vs.* PMSCV.

Figure 5 Gene truncation and partner collaboration regulate the mRNA stability of PAX5 fusion and STK38-PXT1. (**A**) Schematic generation of fusions involving gene truncation and partner collaboration. (**B**) Left: FPKM level of the *PAX5* gene in five PAX5 fusion genes excluding PAX5-ETV6 in the TARGET ALL database. Right: FPKM level of the 5'-terminal genes of five other ETV6 fusion genes except PAX5-ETV6 in the TCGA database. (**C**) Left: FPKM level of the *STK38* gene in six STK38 fusion genes excluding STK38-PXT1 in the TCGA database. Right: FPKM level of 5'-terminal genes of other 5 PXT1 fusion genes except STK38-PXT1 in the TCGA database. (**D**) mRNA half-life of PAX5(WT), PAX5(N) and PAX5-ETV6 in BaF3 cells. (**E**) mRNA half-life of STK38(WT), STK38(N) and STK38-PXT1 in

BaF3 cells. (D, E) Data are represented as mean ± SD (n=3). (B, C, D, E) The significance analysis was conducted using two-tailed unpaired Student's t-test, two-way ANOVA. n.s., $P>0.05$; *, $P<0.05$; **, $P<0.05$; ***, $P<0.001$ *vs.* indicated.

Figure 6 The mRNA stability upregulation of fusion is attributed to enhanced m6A modification. (**A**) The m6A modification level of PAX5(WT), PAX5(N) and PAX5-ETV6 in BaF3 cells. (**B**) The m6A modification level of STK38(WT), STK38(N) and STK38-PXT1 in BaF3 cells. (**C**) mRNA half-life of PAX5-ETV6(WT), PAX5-ETV6(43A→T), and PAX5-ETV6(48A→T) in HEK293T cells. (**D**) The m6A modification level of PAX5-ETV6(WT), PAX5-ETV6(43A→T), and PAX5-ETV6(48A→T) in HEK293T cells. (**E**) mRNA half-life of STK38-PXT1(WT), STK38-PXT1 (708A→T), and STK38-PXT1 (727A→T) in HEK293T cells. (**F**) The m6A modification level of STK38-PXT1(WT), STK38-PXT1 (708A→T), and STK38-PXT1 (727A→T) in HEK293T cells. (A-F) Data are represented as mean ± SD (n=3). (A-F) The significance analysis was conducted using two-tailed paired Student's t-test, one-way or two-way ANOVA analysis. n.s., $P>0.05$; *, $P<0.05$; **, $P<0.01$; ***, $P<0.001$ *vs.* indicated.

Figure 7 m6A reader IGF2BP3 is responsible for maintaining the high stability of fusion mRNA. (**A**) The differential genes of ALL patients with PAX5 fusion. Compared with 657 ALL samples without PAX5 fusions, the differential gene expression volcano plot of 22 ALL samples with PAX5 fusion in the TARGET database. (**B**) The differential genes of ALL patients with STK38-PXT1 fusion. Compared with 168 ALL patients, the differential gene expression volcano plot of 4 patients with STK38-PXT1 fusion in our ALL database. (**C**) The expression levels of IGF2BP3 in ALL samples with different classical oncofusions. (**D**) The effect of shIGF2BP3 on the mRNA half-life of PAX5(WT), PAX5(N) and PAX5-ETV6. (**E**) The effect of shIGF2BP3 on the mRNA half-life of STK38(WT), STK38(N) and STK38-PXT1. (D, E) The mRNA half-life ($t_{1/2}$) was detected by actinomycin D experiment and calculated by simple linear regression. (**F**) The silencing effect of shIgf2bp3 on the BaF3 cells. (**G**) The proliferation-inhibitory effect of shIgf2bp3 on the BaF3 cells overexpressing vector-PMSCV, PAX5(WT), PAX5(N) and PAX5-ETV6. (**H**) The proliferation-inhibitory effect of shIgf2bp3 on the BaF3 cells overexpressing vector-PMSCV, STK38(WT), STK38(N) and STK38-PXT1. (D-H)

Date are represented as mean ± SD (n=3). The significance analysis was conducted using one-way ANOVA or two-way ANOVA analysis. n.s., $P>0.05$; *, $P<0.05$; **, $P<0.01$; ***, $P<0.001$ *vs.* indicated.

Figure 8 Venetoclax specifically inhibits mRNA high-stability fusion-driven ALL. (**A**) Selective sensitivity of BaF3 cell lines overexpressing PAX5-ETV6 to antitumor drugs compared with PAX5(WT). (**B**) Selective sensitivity of BaF3 cell lines overexpressing STK38-PXT1 to antitumor drugs compared with STK38(WT). (A, B) Relative inhibition rate (%): The inhibition ratio of the indicated fusion gene group to the respective wild-type. (**C**) Z-score, the mean sensitivity score, of 23 ALL cell lines to venetoclax. IGF2BP3 Low: Z-score of 9 cell lines with low levels of IGF2BP3 expression, marked in black; IGF2BP3 High: Z-score of the 14 cell lines with high levels of IGF2BP3 expression, marked in red. (**D**) The apoptosis rate-induced by venetoclax in the BaF3 cells overexpressing vector-PMSCV, PAX5(WT) and PAX5-ETV6. (**E**) The apoptosis rate induced by venetoclax in the BaF3 cells overexpressing vector-PMSCV, STK38(WT) and STK38-PXT1. (D-E) Apoptosis of cells induced by 2μM venetoclax was investigated by flow cytometry with Annexin V-PI double staining. (**F**) GSEA Hallmark pathway overlap in PAX5 fusion and STK38-PXT1-positive ALL. Left: Venn diagram of significantly enriched Hallmark gene sets in PAX5 fusion-positive versus fusion-negative patients and in STK38-PXT1-positive versus fusion-negative patients. Right: Shared Hallmark pathways uniquely enriched in both fusion-positive groups, displayed with normalized enrichment scores (NES) for each comparison; color intensity reflects statistical significance ($-\log_{10}$ P-value). (**G**) GSEA enrichment plots for the HALLMARK_OXIDATIVE_PHOSPHORYLATION pathway in PAX5 fusion-positive versus fusion-negative patients and STK38-PXT1-positive versus fusion-negative patients. **(H-I)** *In vivo* antileukemic activity of venetoclax in NSG mouse models of PAX5-ETV6- and STK38-PXT1-driven leukemia. NSG mice were intravenously engrafted with BaF3 cells overexpressing PAX5-ETV6 or STK38-PXT1, and treated with venetoclax (100 mg/kg/day by oral gavage) (n=5 per group). (H) Percentages of $mCD19^+$ cells in peripheral blood at day 45 after transplantation. (I) Kaplan-Meier curves for overall survival. (D, E) Data are represented as mean ± SD (n=3). (C, D, E, H, I) The significance analysis was conducted using two-tailed unpaired Student's t-test, two-way ANOVA or log-rank test. n.s., $P>0.05$; *, $P<0.05$;

***, $P<0.001$ *vs.* indicated; #, $P<0.05$; ##, $P<0.01$; ###, $P<0.001$ *vs.* indicated.

Figure 1

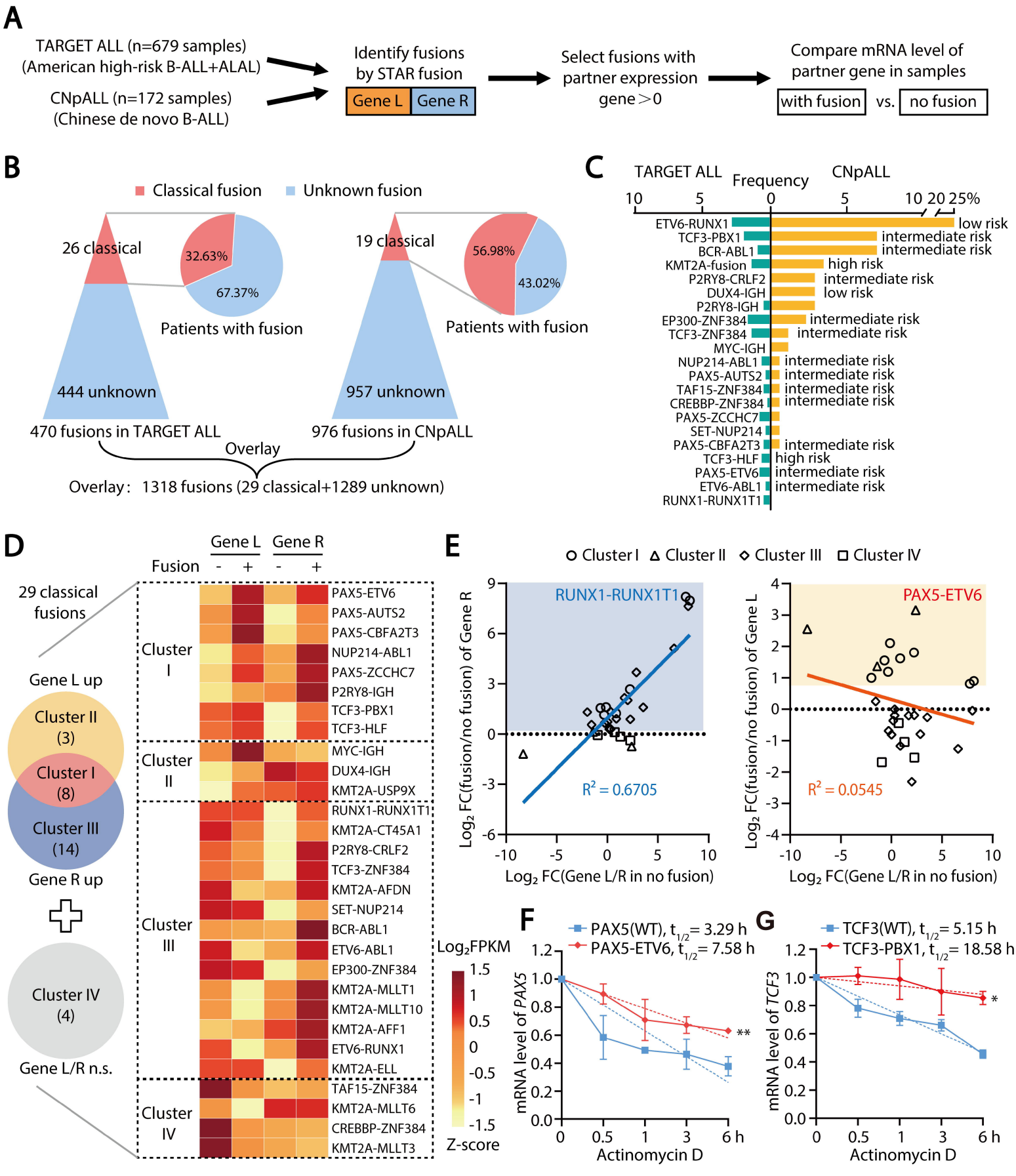
A
TARGET ALL (n=679 samples)
(American high-risk B-ALL+ALAL)
CNpALL (n=172 samples)
(Chinese de novo B-ALL)
Identify fusions by STAR fusion
Gene L
Gene R
Select fusions with partner expression gene>0
Compare mRNA level of partner gene in samples
with fusion
vs.
no fusion
B
Classical fusion
Unknown fusion
26 classical
32.63%
67.37%
Patients with fusion
444 unknown
470 fusions in TARGET ALL
19 classical
56.98%
43.02%
Patients with fusion
957 unknown
976 fusions in CNpALL
Overlay
Overlay: 1318 fusions (29 classical+1289 unknown)
C
TARGET ALL
Frequency
CNpALL
10 5 0 5 10 20 25%
ETV6-RUNX1 low risk
TCF3-PBX1 intermediate risk
BCR-ABL1 intermediate risk
KMT2A-fusion high risk
P2RY8-CRLF2 intermediate risk
DUX4-IGH low risk
P2RY8-IGH
EP300-ZNF384 intermediate risk
TCF3-ZNF384 intermediate risk
MYC-IGH
NUP214-ABL1 intermediate risk
PAX5-AUTS2 intermediate risk
TAF15-ZNF384 intermediate risk
CREBBP-ZNF384 intermediate risk
PAX5-ZCCHC7
SET-NUP214
PAX5-CBFA2T3 intermediate risk
TCF3-HLF high risk
PAX5-ETV6 intermediate risk
ETV6-ABL1 intermediate risk
RUNX1-RUNX1T1
D
Gene L
Gene R
Fusion - + - +
29 classical fusions
Gene L up
Cluster II (3)
Cluster I (8)
Cluster III (14)
Gene R up
Cluster IV (4)
Gene L/R n.s.
Cluster I
PAX5-ETV6
PAX5-AUTS2
PAX5-CBFA2T3
NUP214-ABL1
PAX5-ZCCHC7
P2RY8-IGH
TCF3-PBX1
TCF3-HLF
Cluster II
MYC-IGH
DUX4-IGH
KMT2A-USP9X
Cluster III
RUNX1-RUNX1T1
KMT2A-CT45A1
P2RY8-CRLF2
TCF3-ZNF384
KMT2A-AFDN
SET-NUP214
BCR-ABL1
ETV6-ABL1
EP300-ZNF384
KMT2A-MLLT1
KMT2A-MLLT10
KMT2A-AFF1
ETV6-RUNX1
KMT2A-ELL
Cluster IV
TAF15-ZNF384
KMT2A-MLLT6
CREBBP-ZNF384
KMT2A-MLLT3
Log2FPKM
1.5 1 0.5 0 -0.5 -1 -1.5
Z-score
E
Cluster I Cluster II Cluster III Cluster IV
RUNX1-RUNX1T1
Log2 FC(fusion/no fusion) of Gene R
R2 = 0.6705
Log2 FC(Gene L/R in no fusion)
PAX5-ETV6
Log2 FC(fusion/no fusion) of Gene L
R2 = 0.0545
Log2 FC(Gene L/R in no fusion)
F
PAX5(WT), t1/2= 3.29 h
PAX5-ETV6, t1/2= 7.58 h
mRNA level of PAX5
**
Actinomycin D
G
TCF3(WT), t1/2= 5.15 h
TCF3-PBX1, t1/2= 18.58 h
mRNA level of TCF3
*
Actinomycin D

Figure 2

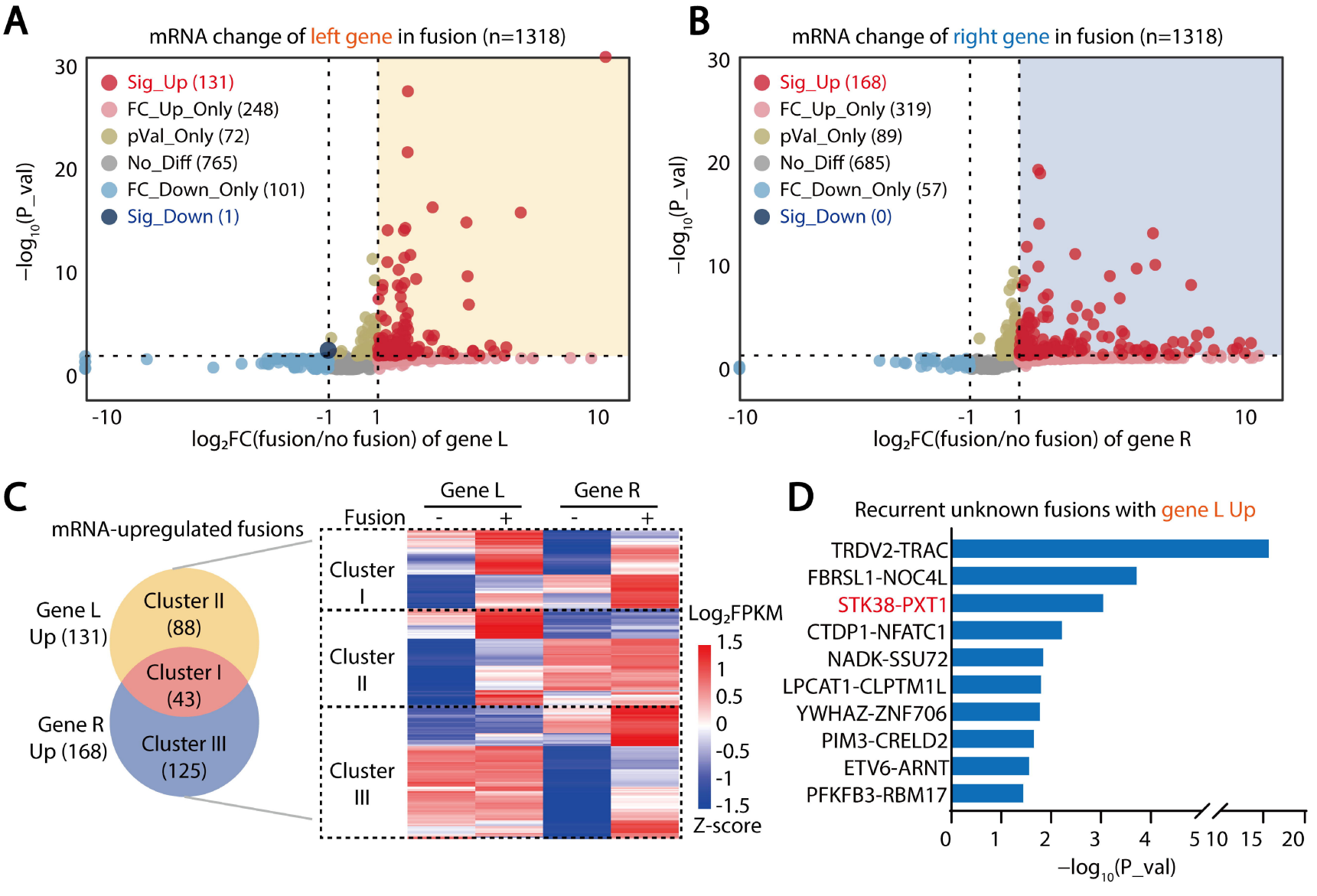
A
mRNA change of left gene in fusion (n=1318)
Sig_Up (131)
FC_Up_Only (248)
pVal_Only (72)
No_Diff (765)
FC_Down_Only (101)
Sig_Down (1)
−log10(P_val)
log2FC(fusion/no fusion) of gene L
B
mRNA change of right gene in fusion (n=1318)
Sig_Up (168)
FC_Up_Only (319)
pVal_Only (89)
No_Diff (685)
FC_Down_Only (57)
Sig_Down (0)
−log10(P_val)
log2FC(fusion/no fusion) of gene R
C
mRNA-upregulated fusions
Gene L Up (131)
Gene R Up (168)
Cluster II (88)
Cluster I (43)
Cluster III (125)
Fusion
Gene L
Gene R
Cluster I
Cluster II
Cluster III
Log2FPKM
Z-score
D
Recurrent unknown fusions with gene L Up
TRDV2-TRAC
FBRSL1-NOC4L
STK38-PXT1
CTDP1-NFATC1
NADK-SSU72
LPCAT1-CLPTM1L
YWHAZ-ZNF706
PIM3-CRELD2
ETV6-ARNT
PFKFB3-RBM17
−log10(P_val)

Figure 3

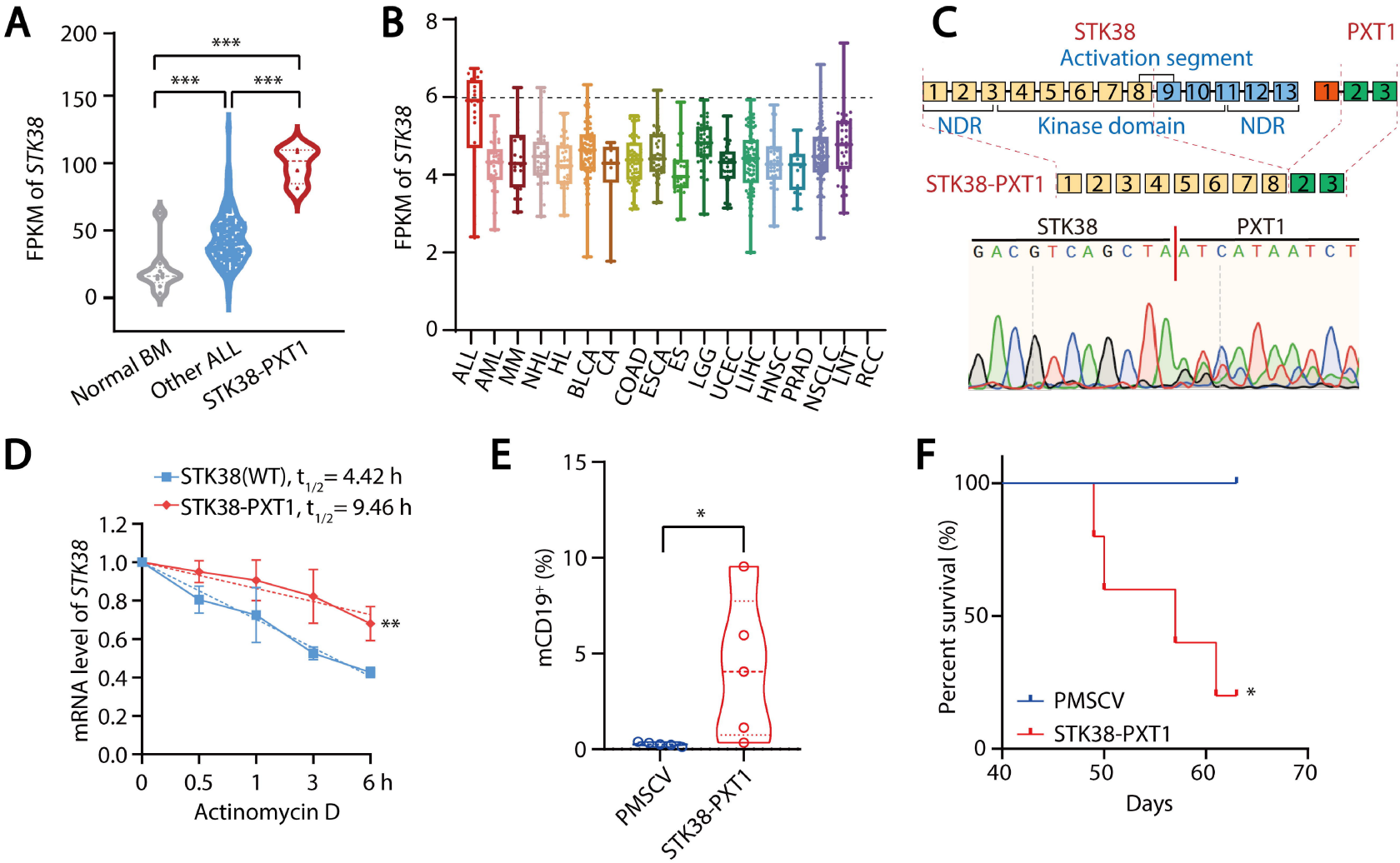
A
FPKM of STK38
200
150
100
50
0
***
***
***
Normal BM
Other ALL
STK38-PXT1
B
FPKM of STK38
8
6
4
2
0
ALL
AML
MM
NHL
HL
BLCA
CA
COAD
ESCA
ES
LGG
UCEC
LIHC
HNSC
PRAD
NSCLC
LNT
RCC
C
STK38
PXT1
Activation segment
1 2 3 4 5 6 7 8 9 10 11 12 13
1 2 3
NDR
Kinase domain
NDR
STK38-PXT1
1 2 3 4 5 6 7 8 2 3
STK38
PXT1
G A C G T C A G C T A A T C A T A A T C T
D
STK38(WT), t1/2= 4.42 h
STK38-PXT1, t1/2= 9.46 h
mRNA level of STK38
1.2
1.0
0.8
0.6
0.4
0.2
0.0
**
0
0.5
1
3
6 h
Actinomycin D
E
mCD19+ (%)
15
10
5
0
*
PMSCV
STK38-PXT1
F
Percent survival (%)
100
50
0
PMSCV
STK38-PXT1
*
40
50
60
70
Days

Figure 4

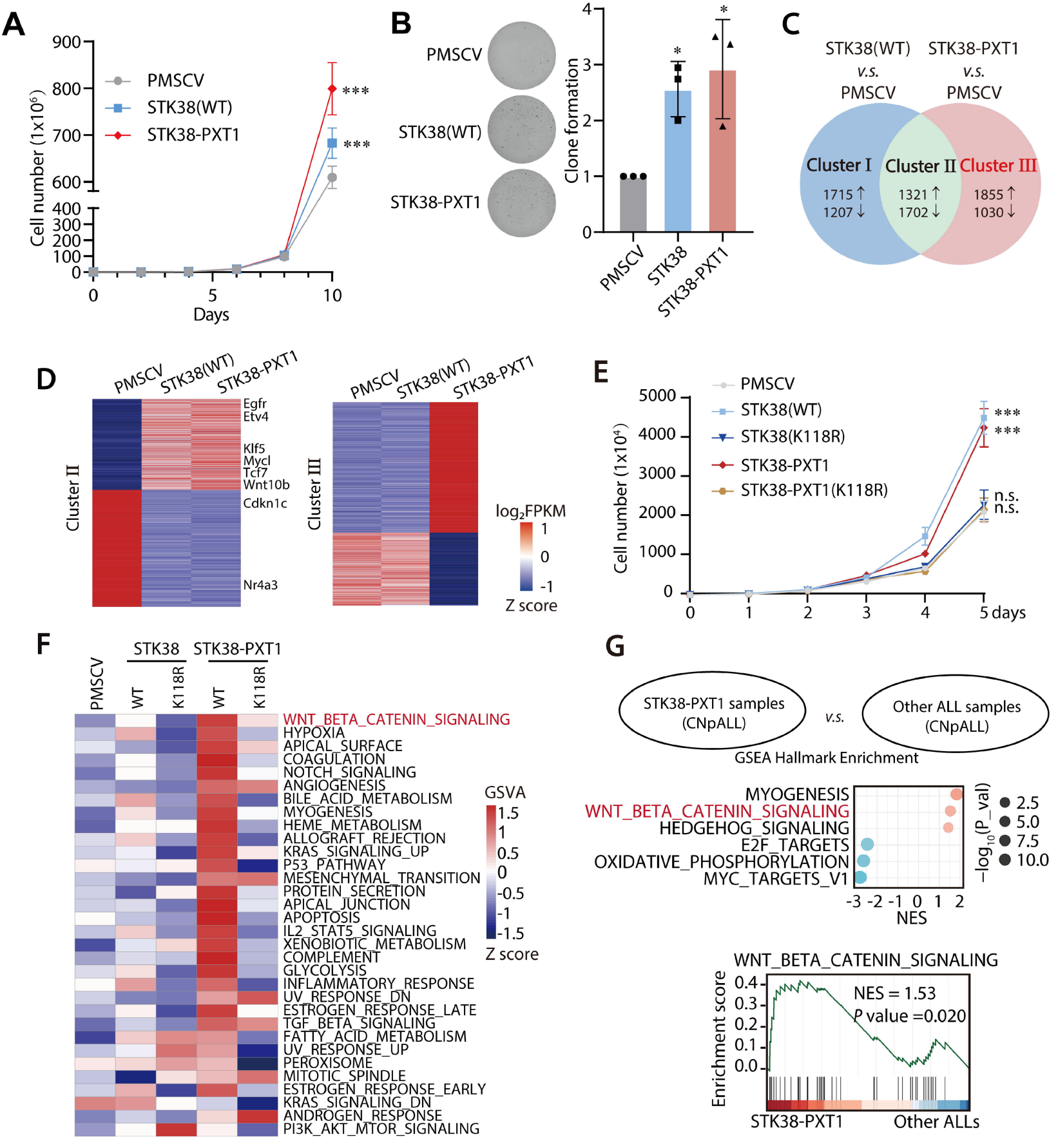
A
Cell number (1x10⁶)
PMSCV
STK38(WT)
STK38-PXT1
***
***
Days
B
PMSCV
STK38(WT)
STK38-PXT1
Clone formation
PMSCV
STK38
STK38-PXT1
C
STK38(WT) v.s. PMSCV
STK38-PXT1 v.s. PMSCV
Cluster I
1715 ↑
1207 ↓
Cluster II
1321 ↑
1702 ↓
Cluster III
1855 ↑
1030 ↓
D
PMSCV
STK38(WT)
STK38-PXT1
Cluster II
Egfr
Etv4
Klf5
Mycl
Tcf7
Wnt10b
Cdkn1c
Nr4a3
Cluster III
log2FPKM
Z score
E
Cell number (1x10⁴)
PMSCV
STK38(WT)
STK38(K118R)
STK38-PXT1
STK38-PXT1(K118R)
***
***
n.s.
n.s.
5 days
F
PMSCV
STK38
STK38-PXT1
WT
K118R
WT
K118R
WNT_BETA_CATENIN_SIGNALING
HYPOXIA
APICAL_SURFACE
COAGULATION
NOTCH_SIGNALING
ANGIOGENESIS
BILE_ACID_METABOLISM
MYOGENESIS
HEME_METABOLISM
ALLOGRAFT_REJECTION
KRAS_SIGNALING_UP
P53_PATHWAY
MESENCHYMAL_TRANSITION
PROTEIN_SECRETION
APICAL_JUNCTION
APOPTOSIS
IL2_STAT5_SIGNALING
XENOBIOTIC_METABOLISM
COMPLEMENT
GLYCOLYSIS
INFLAMMATORY_RESPONSE
UV_RESPONSE_DN
ESTROGEN_RESPONSE_LATE
TGF_BETA_SIGNALING
FATTY_ACID_METABOLISM
UV_RESPONSE_UP
PEROXISOME
MITOTIC_SPINDLE
ESTROGEN_RESPONSE_EARLY
KRAS_SIGNALING_DN
ANDROGEN_RESPONSE
PI3K_AKT_MTOR_SIGNALING
GSVA
Z score
G
STK38-PXT1 samples (CNpALL)
v.s.
Other ALL samples (CNpALL)
GSEA Hallmark Enrichment
MYOGENESIS
WNT_BETA_CATENIN_SIGNALING
HEDGEHOG_SIGNALING
E2F_TARGETS
OXIDATIVE_PHOSPHORYLATION
MYC_TARGETS_V1
NES
−log10(P_val)
WNT_BETA_CATENIN_SIGNALING
NES = 1.53
P value =0.020
Enrichment score
STK38-PXT1
Other ALLs

Figure 5

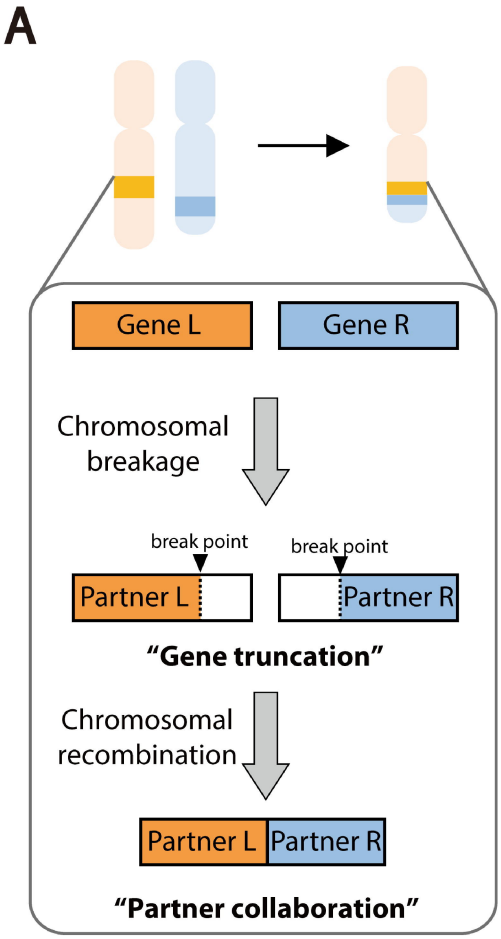
A
Gene L
Gene R
Chromosomal breakage
break point
break point
Partner L
Partner R
"Gene truncation"
Chromosomal recombination
Partner L
Partner R
"Partner collaboration"

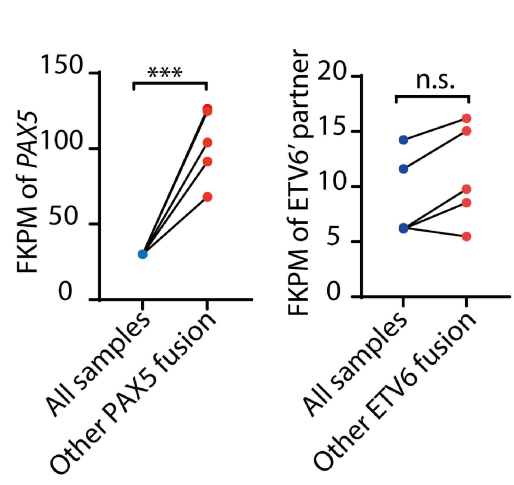
B
FKPM of PAX5
150
100
50
0
***
All samples
Other PAX5 fusion
FKPM of ETV6' partner
20
15
10
5
0
n.s.
All samples
Other ETV6 fusion

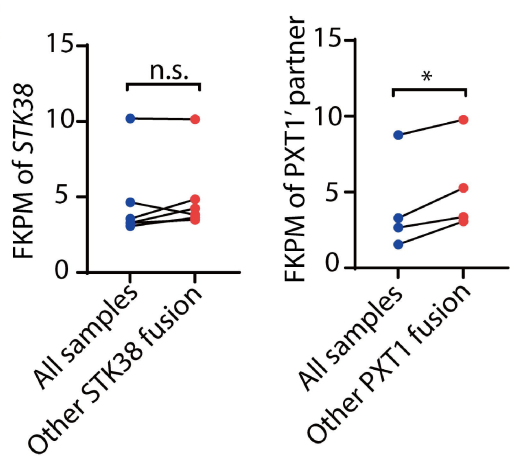
C
FKPM of STK38
15
10
5
0
n.s.
All samples
Other STK38 fusion
FKPM of PXT1' partner
15
10
5
0
*
All samples
Other PXT1 fusion

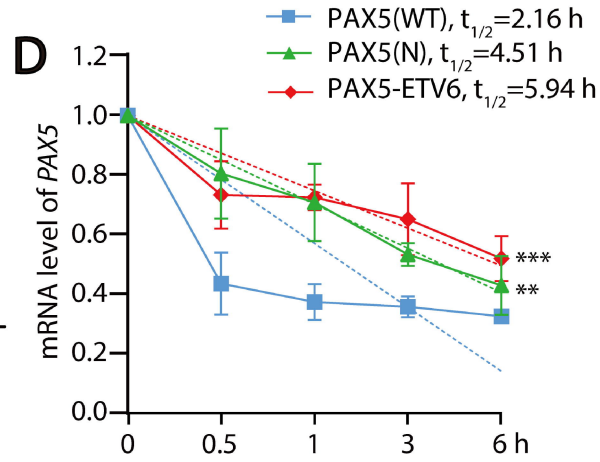
D
PAX5(WT), t1/2=2.16 h
PAX5(N), t1/2=4.51 h
PAX5-ETV6, t1/2=5.94 h
mRNA level of PAX5
1.2
1.0
0.8
0.6
0.4
0.2
0.0
0
0.5
1
3
6 h
***
**

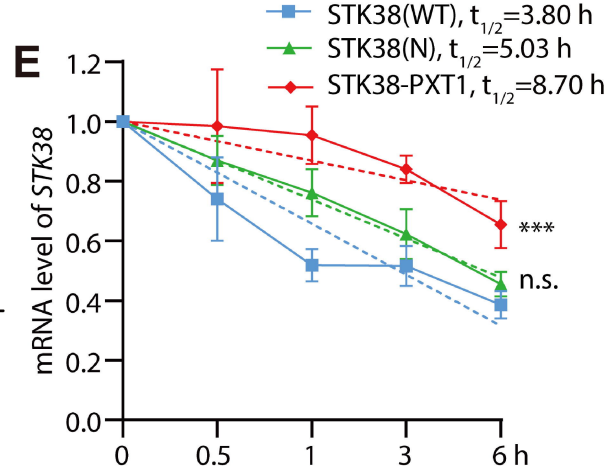
E
STK38(WT), t1/2=3.80 h
STK38(N), t1/2=5.03 h
STK38-PXT1, t1/2=8.70 h
mRNA level of STK38
1.2
1.0
0.8
0.6
0.4
0.2
0.0
0
0.5
1
3
6 h
***
n.s.

Figure 6

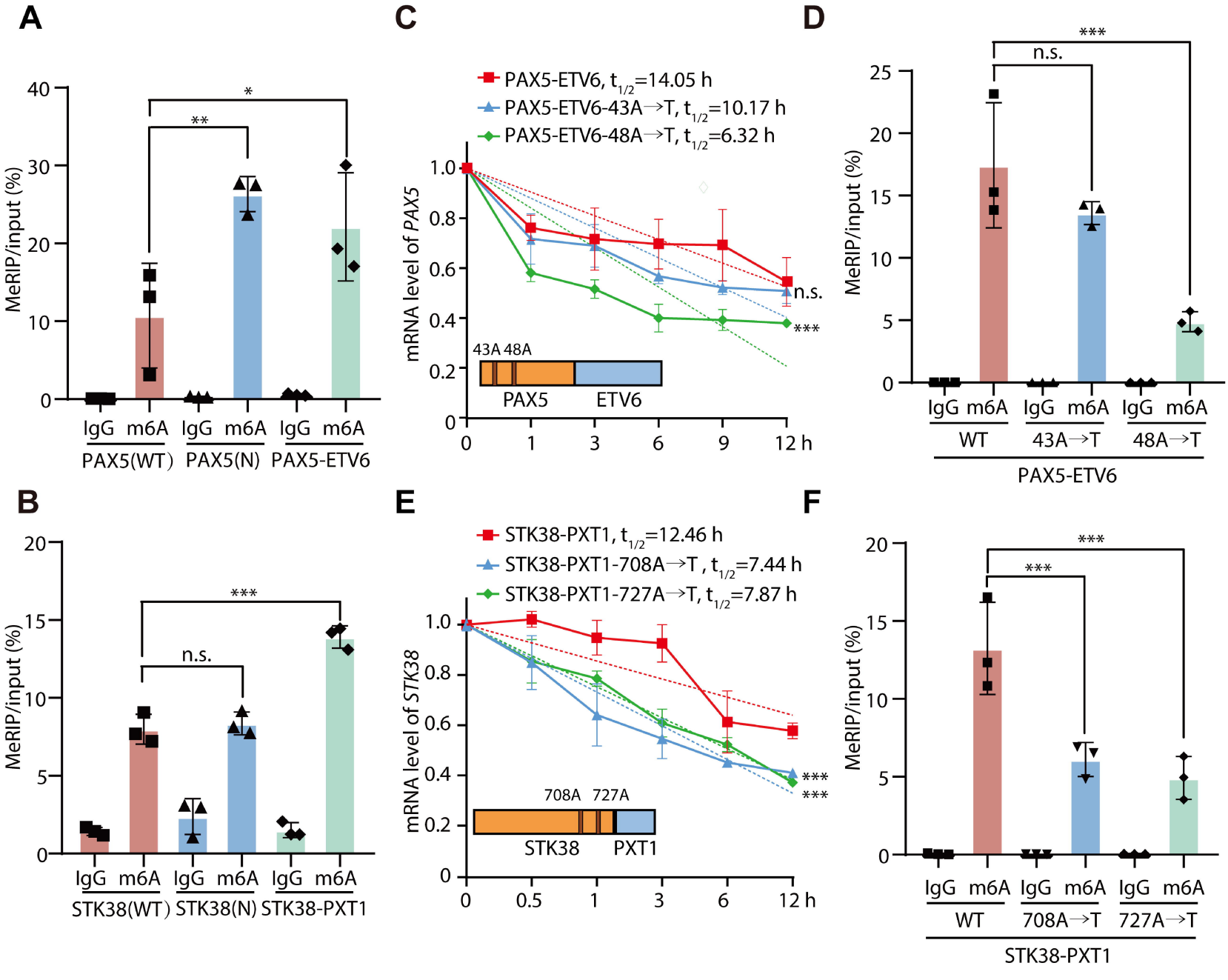
A
MeRIP/input (%)
IgG m6A IgG m6A IgG m6A
PAX5(WT) PAX5(N) PAX5-ETV6
B
MeRIP/input (%)
n.s.
IgG m6A IgG m6A IgG m6A
STK38(WT) STK38(N) STK38-PXT1
C
PAX5-ETV6, t1/2=14.05 h
PAX5-ETV6-43A→T, t1/2=10.17 h
PAX5-ETV6-48A→T, t1/2=6.32 h
mRNA level of PAX5
n.s.
43A 48A
PAX5 ETV6
E
STK38-PXT1, t1/2=12.46 h
STK38-PXT1-708A→T , t1/2=7.44 h
STK38-PXT1-727A→T, t1/2=7.87 h
mRNA level of STK38
708A 727A
STK38 PXT1
D
MeRIP/input (%)
n.s.
IgG m6A IgG m6A IgG m6A
WT 43A→T 48A→T
PAX5-ETV6
F
MeRIP/input (%)
IgG m6A IgG m6A IgG m6A
WT 708A→T 727A→T
STK38-PXT1

Figure 7

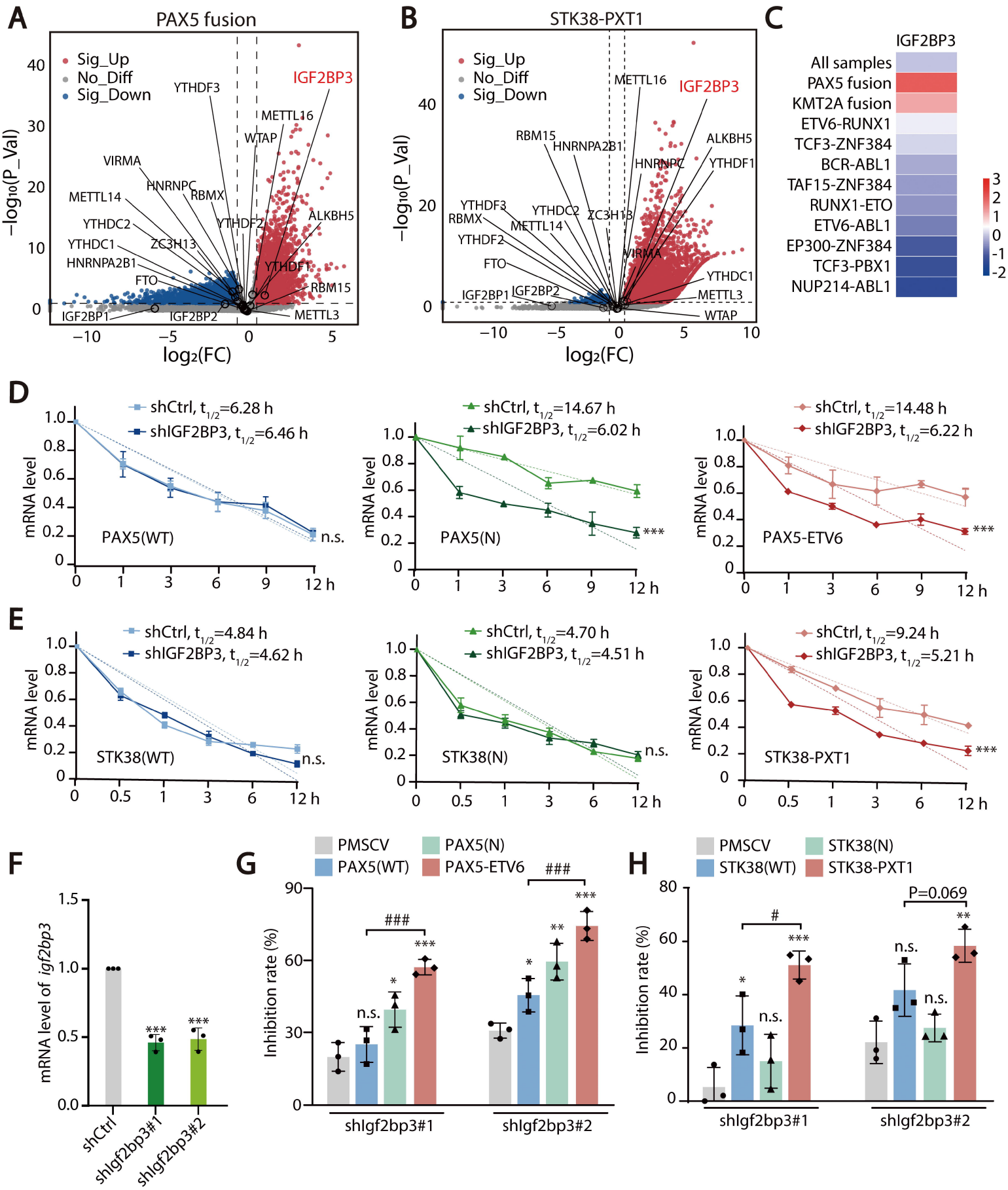
A
PAX5 fusion
Sig_Up
No_Diff
Sig_Down
IGF2BP3
YTHDF3
METTL16
WTAP
VIRMA
HNRNPC
RBMX
METTL14
YTHDF2
ALKBH5
YTHDC2
YTHDC1
ZC3H13
HNRNPA2B1
YTHDF1
FTO
RBM15
IGF2BP1
IGF2BP2
METTL3
−log10(P_Val)
log2(FC)
B
STK38-PXT1
Sig_Up
No_Diff
Sig_Down
METTL16
IGF2BP3
RBM15
HNRNPA2B1
ALKBH5
HNRNPC
YTHDF1
YTHDF3
YTHDC2
ZC3H13
RBMX
METTL14
YTHDF2
VIRMA
FTO
YTHDC1
IGF2BP1
IGF2BP2
METTL3
WTAP
−log10(P_Val)
log2(FC)
C
IGF2BP3
All samples
PAX5 fusion
KMT2A fusion
ETV6-RUNX1
TCF3-ZNF384
BCR-ABL1
TAF15-ZNF384
RUNX1-ETO
ETV6-ABL1
EP300-ZNF384
TCF3-PBX1
NUP214-ABL1
D
shCtrl, t1/2=6.28 h
shIGF2BP3, t1/2=6.46 h
PAX5(WT)
n.s.
shCtrl, t1/2=14.67 h
shIGF2BP3, t1/2=6.02 h
PAX5(N)
***
shCtrl, t1/2=14.48 h
shIGF2BP3, t1/2=6.22 h
PAX5-ETV6
***
mRNA level
E
shCtrl, t1/2=4.84 h
shIGF2BP3, t1/2=4.62 h
STK38(WT)
n.s.
shCtrl, t1/2=4.70 h
shIGF2BP3, t1/2=4.51 h
STK38(N)
n.s.
shCtrl, t1/2=9.24 h
shIGF2BP3, t1/2=5.21 h
STK38-PXT1
***
mRNA level
F
mRNA level of igf2bp3
shCtrl
shIgf2bp3#1
shIgf2bp3#2
G
PMSCV
PAX5(WT)
PAX5(N)
PAX5-ETV6
###
###
Inhibition rate (%)
shIgf2bp3#1
shIgf2bp3#2
H
PMSCV
STK38(WT)
STK38(N)
STK38-PXT1
#
P=0.069
Inhibition rate (%)
shIgf2bp3#1
shIgf2bp3#2

Figure 8

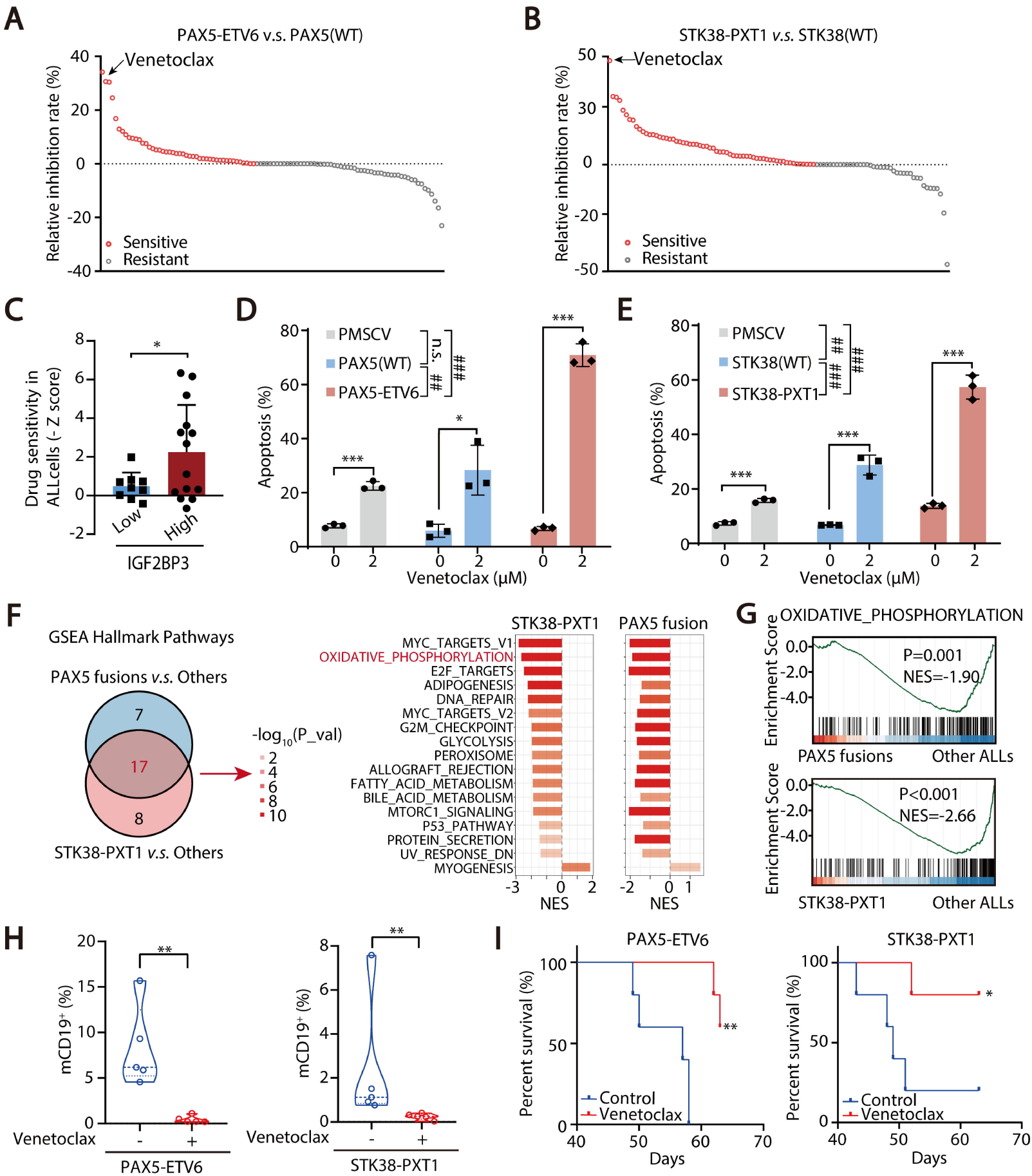
A
PAX5-ETV6 v.s. PAX5(WT)
Venetoclax
Relative inhibition rate (%)
Sensitive
Resistant
B
STK38-PXT1 v.s. STK38(WT)
Venetoclax
Relative inhibition rate (%)
Sensitive
Resistant
C
Drug sensitivity in ALLcells (- Z score)
Low
High
IGF2BP3
D
PMSCV
PAX5(WT)
PAX5-ETV6
Apoptosis (%)
Venetoclax (μM)
E
PMSCV
STK38(WT)
STK38-PXT1
Apoptosis (%)
Venetoclax (μM)
F
GSEA Hallmark Pathways
PAX5 fusions v.s. Others
STK38-PXT1 v.s. Others
-log10(P_val)
STK38-PXT1
PAX5 fusion
MYC_TARGETS_V1
OXIDATIVE_PHOSPHORYLATION
E2F_TARGETS
ADIPOGENESIS
DNA_REPAIR
MYC_TARGETS_V2
G2M_CHECKPOINT
GLYCOLYSIS
PEROXISOME
ALLOGRAFT_REJECTION
FATTY_ACID_METABOLISM
BILE_ACID_METABOLISM
MTORC1_SIGNALING
P53_PATHWAY
PROTEIN_SECRETION
UV_RESPONSE_DN
MYOGENESIS
NES
NES
G
OXIDATIVE_PHOSPHORYLATION
Enrichment Score
P=0.001
NES=-1.90
PAX5 fusions
Other ALLs
Enrichment Score
P<0.001
NES=-2.66
STK38-PXT1
Other ALLs
H
mCD19+ (%)
Venetoclax
PAX5-ETV6
mCD19+ (%)
Venetoclax
STK38-PXT1
I
PAX5-ETV6
Percent survival (%)
Control
Venetoclax
Days
STK38-PXT1
Percent survival (%)
Control
Venetoclax
Days

Supplementary information

Supplementary materials and methods

Cells and cell culture

Human embryonic kidney HEK293T cell lines were provided by Invitrogen (Grand Island, NY). The mouse pro-B cell line BaF3 was purchased from the Shanghai Institute of JIHE SHENG WU KEJI Biology (Shanghai, China). Human NALM-6 cell lines was purchased were purchased from the American Type Culture Collection (Rockville, USA). Human REH cell lines was purchased from the Shanghai Institute of Biochemistry and Cell Biology (Shanghai, China). Human HEK293T cells were cultured in DMEM medium. BaF3 cells were cultured in RPMI 1640 medium supplemented with 2 ng/mL IL-3. NALM-6 and REH cells were cultured in RPMI 1640 medium. All medium were supplemented with 10% fetal bovine serum (Gibco BRL) and 1% penicillin/streptomycin. Cells were cultured in an incubator at 37°C with 5% CO_2. All cell lines were routinely tested for mycoplasma using Mycoplasma Detection Kit (Bimake, Houston, TX, USA) and passaged for a maximum of two months. All cell lines were authenticated utilizing short tandem repeat (STR) profiling every 6 months.

Plasmids and reagents

The coding sequences of PAX5-ETV6 and STK38-PXT1 were subcloned into the pCDH-MSCV-GFP (PMSCV) plasmid. shRNA sequences for human IGF2BP3 and mouse Igf2bp3 were cloned to pLKO.1 vector. The targeting sequences are as follows: shIGF2BP3, TCTGCGGCTTGTAAGTCTATT; shIgf2bp3#1, CGCGGAGAAGTCCATTACTAT; shIgf2bp3#2, CCTACCCACAATTTGAGCAAT. The primers used for PCR identification in animal studies are as follows: STK38-PXT1-F: 5'-ATGGCAATGACAGGCTCAAC-3', STK38-PXT1-R: 5'-TTATTTCCTCCTGGTGATGC-3'. The packaging plasmid pRΔ8.9 and envelope plasmid pMD.G were kindly provided by Dr. D.B. Kohn (University of Southern California). 102 FDA-approved antitumor drugs including venetoclax, as well as actinomycin D, were purchased from Selleck Chemicals (Houston, Texas).

The fusion and gene expression analysis of ALL samples

First, the patient-derived ALL cells from bone marrow were obtained, and the RNA-seq detection was performed by Shanghai Tissue bank Biotechnology Co., Ltd. Then the STAR-

Fusion v1.7.0 was used to identify fusions from RNA-seq data across ALL samples in our CNpALL cohort.

Cellular proliferation, colony formation and cell apoptosis analysis

The total cell number was determined by trypan blue exclusion with manual counting in Burker chambers. The cell colony formation ability was detected by soft agar (Sigma, Shanghai) colony formation. We used Nitrotetrazolium Blue chloride (Aladdin, Shanghai) to color the cell clones. The apoptosis quantification was detected by PI/Annexin V-staining, and Annexin V-stained cells were analyzed to measure the cell apoptosis rate.

The mRNA half-life detection

The target gene was transfected into HEK293T or BaF3 cells, then actinomycin D (5 μg/mL, Apexbio) was used to block de novo RNA synthesis. Samples are collected at different time points after the addition of actinomycin D for mRNA extraction. Specific PCR primers were used to detect the expression levels of the corresponding mRNA (**Table S1**). Half-life ($t_{1/2}$): the time required for the relative expression level of mRNA to decrease to half. Simple linear regression was used to calculate the half-life of mRNA.

RNA sequencing assay of BaF3 cells

The sequencing of samples based on BaF3 cells was entrusted to Shanghai Biochip Co., Ltd. The first step of transcriptome sequencing (RNA-seq) involved extracting RNA from cells and enriching for target RNA, then converting the RNA into complementary DNA (cDNA), fragmenting it, and ligating adapters. Finally, these adapters were sequenced on the Illumina HiSeq 2000 platform for analysis.

Quantitative real-time PCR

Total RNA was isolated from cells with Trizol reagent (Invitrogen), and cDNA was transcribed using a transcript kit (TransGen Biotech). qRT-PCR analysis was performed using the SYBR Green (Bio-Rad) method on the QuantStudio 6 (Thermo). The gene expression was normalized to the expression of the gene encoding GAPDH. Sequences of the primers for qRT-PCR are shown in **Table S1**. Expression levels were normalized to the GAPDH mRNA level using the $2^{-\Delta\Delta Ct}$ method.

MERIP-qPCR experimental procedure

The target gene was transfected into HEK293T or BaF3 cells. Extract the mRNA required for the experiment, using non-fragmented mRNA for detection. Retain 10% of the mRNA sample as input, and the remaining sample was subjected to IP with m6A-specific antibody. Mix 15 μL of Magnetic Beads A/G Blend, RNasin Plus RNase inhibitor (40 U/μL), 300 μg of mRNA sample, 200 μL of IP buffer, and 25 μL of m6A-specific antibody. Incubate at 4°C with end-over-end rotation for 4 hours, followed by washing 4 times. Add 100 μL of elution buffer to the magnetic beads, and incubate the mixture continuously at 4°C with shaking for 4 hours. Finally, the washed mRNA was detected for content using qPCR. Detail primers are shown in **Table S1**.

Supplementary figures

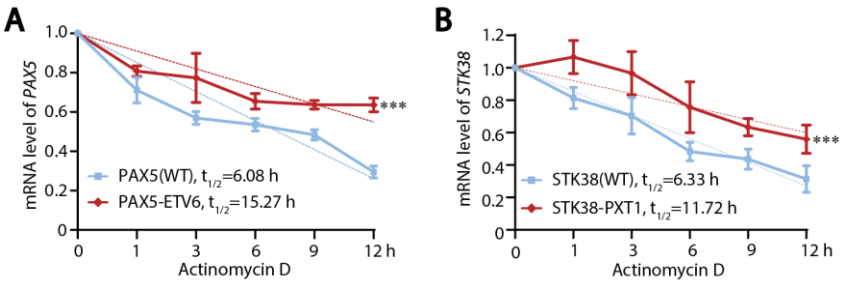

Figure S1. mRNA half-lives for PAX5-ETV6 and STK38-PXT1 versus wild type. (**A**) The mRNA half-life of PAX5(WT) and PAX5-ETV6. Fusions were overexpressed in HEK293T cells by plasmid transfection. After 24h, actinomycin D inhibited mRNA synthesis by 5 μg/mL. Samples were collected to extract mRNA at the indicated times after being treated with actinomycin. $t_{1/2}$ was calculated by Simple Linear Regression. (**B**) The mRNA half-life of STK38(WT) and STK38-PXT1. (A, B) Data are represented as mean ± SD (n=3). The significance analysis was conducted by two-way ANOVA analysis. ***, $P<0.001$ *vs.* indicated.

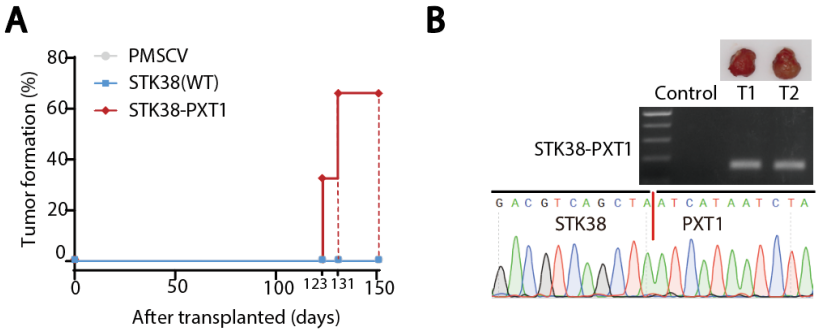

Figure S2. The effect of STK38-PXT1 fusion on BaF3 xenograft tumorigenicity. (**A**) The oncogenic transformation activity of STK38-PXT1 fusion. BaF3 cells transduced with vector-PMSCV virus, STK38(WT) and STK38-PXT1 were subcutaneously injected into nude mice. (**B**) Identification of STK38-PXT1 in transplanted tumors. After 150 days post-transplantation, all mice were euthanized, and tumors were excised for photography; mice without tumor formation were represented by a segment of their tail. Then the tumors were extracted for RNA isolation and the presence of STK38-PXT1 was detected by RT-PCR.

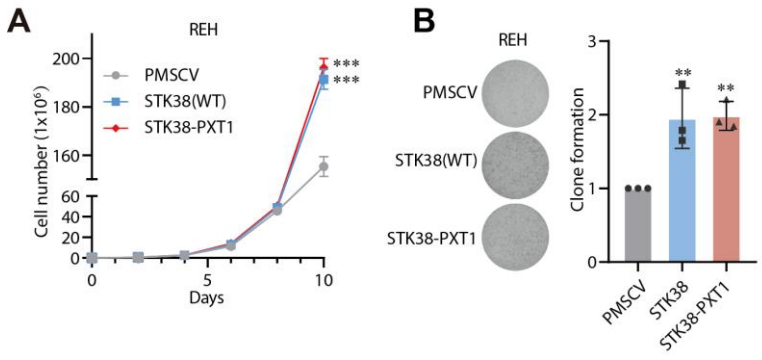

Figure S3. The effect of STK38-PXT1 on REH cell proliferation and colony formation. (**A**) Proliferation curve of REH cells overexpressing STK38 (WT), STK38-PXT1. REH cells were transfected with lentivirus PMSCV, STK38 (WT), STK38-PXT1. (**B**) The clonality of REH cells overexpressing STK38 (WT), STK38-PXT1. (A, B) Data are represented as mean ± SD (n=3). (A) The significance analysis was conducted by two-way ANOVA analysis. ***, *P*<0.001 *vs.* PMSCV. (B) The significance analysis was conducted by one-way ANOVA analysis. **, *P*<0.01 *vs.* PMSCV.

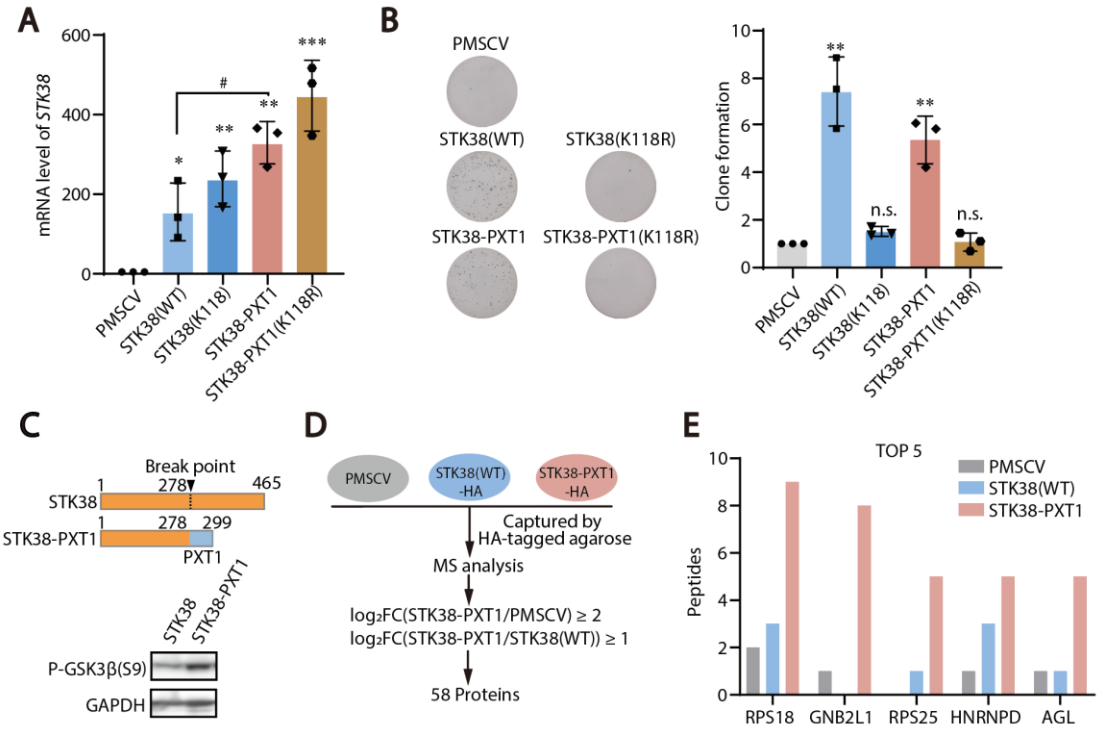

Figure S4. The effect of STK38-PXT1 overexpression on leukemogenesis and underlying potential mechanisms (**A**) The mRNA level of STK38 in the BaF3 cells overexpressing STK38-PXT1. (**B**) The clonality of BaF3 cells overexpressing STK38-PXT1. (A, B) BaF3 cells were transfected with lentivirus PMSCV, STK38 (WT), STK38(K118R), STK38-PXT1, and

STK38-PXT1(K118R). (**C**) p-GSK3β (Ser9) of BaF3 cells expressing STK38(WT) or STK38-PXT1. (**D**) Workflow for the identification of STK38(WT) and STK38-PXT1 interaction proteins. HEK293T cells were transfected with PMSCV, STK38(WT)-HA, or STK38-PXT1-HA. Lysates were captured with HA-tagged agarose and analyzed by LC-MS/MS. Candidate STK38-PXT1-preferential interactors were defined by $\log_2$(STK38-PXT1/PMSCV) ≥ 2 and $\log_2$(STK38-PXT1/STK38 (WT)) ≥ 1. (**E**) Peptide counts for the top five STK38-PXT1-preferential interactors identified by MS across PMSCV, STK38(WT), and STK38-PXT1 samples. (A, B) Data are represented as mean ± SD (n=3). The significance analysis was conducted by one-way ANOVA analysis. n.s., P>0.05; *, *P*<0.05; **, *P*<0.01; ***, *P*<0.001 *vs.* PMSCV. #, *P*<0.05 *vs.* indicated.

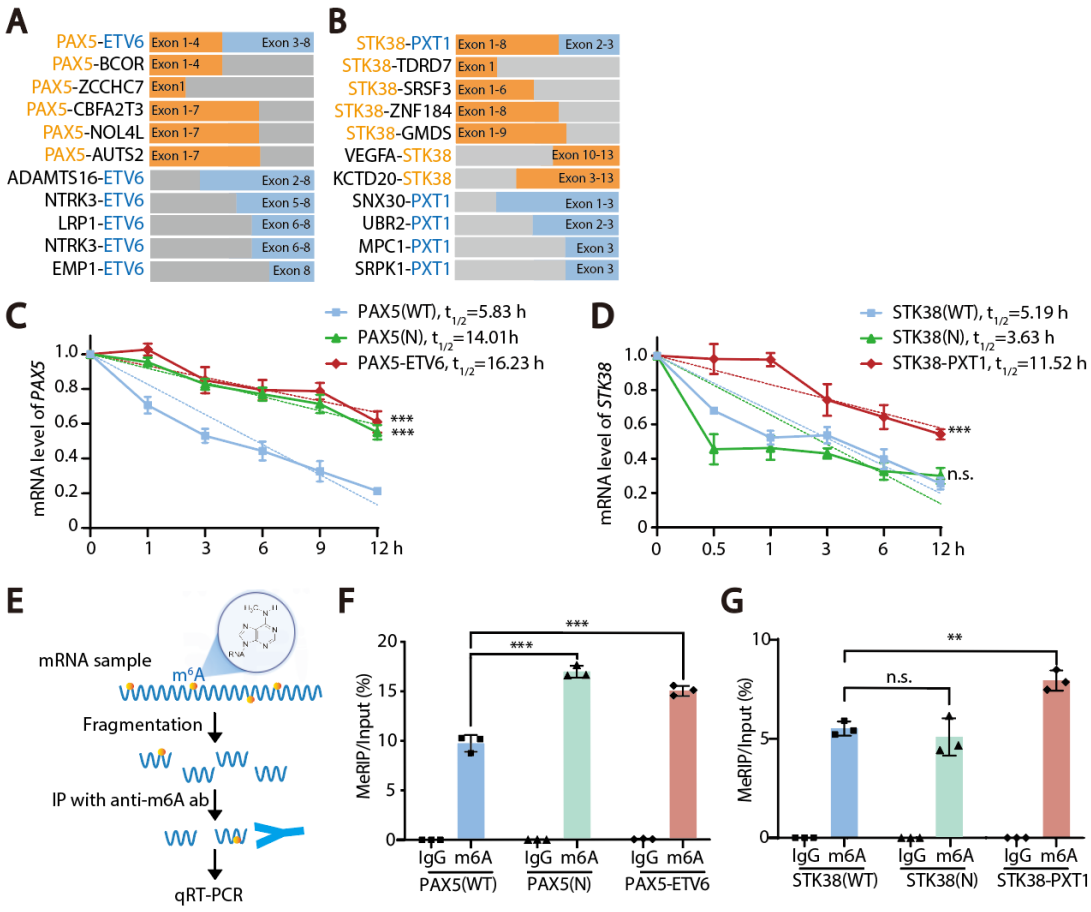

Figure S5. The mRNA half-life and m6A modification of PAX5 fusion and STK38-PXT1. (**A**) Structural schematic diagram of PAX5 fusions from pan-cancer database. (**B**) Structural schematic diagram of STK38 fusions from pan-cancer database. (**C**) mRNA half-life of

PAX5(WT), PAX5(N) and PAX5-ETV6 in HEK293T cell. (**D**) mRNA half-life of STK38(WT), STK38(N) and STK38-PXT1 in HEK293T cell. (**E**) Schematic diagram of MeRIP-qPCR process. (**F**) The m6A modification level of PAX5(WT), PAX5(N) and PAX5-ETV6 in HEK293T cell. (**G**) The m6A modification level of STK38(WT), STK38(N) and STK38-PXT1 in HEK293T cell. (C, D) The significance analysis was conducted by two-way ANOVA analysis. n.s., $P>0.05$; ***, $P<0.001$ *vs.* PAX5(WT) (C) and STK38(WT) (D). (F, G) The significance analysis was conducted by one-way ANOVA analysis. n.s., $P>0.05$; **, $P<0.01$, ***, $P<0.001$ *vs.* indicated.

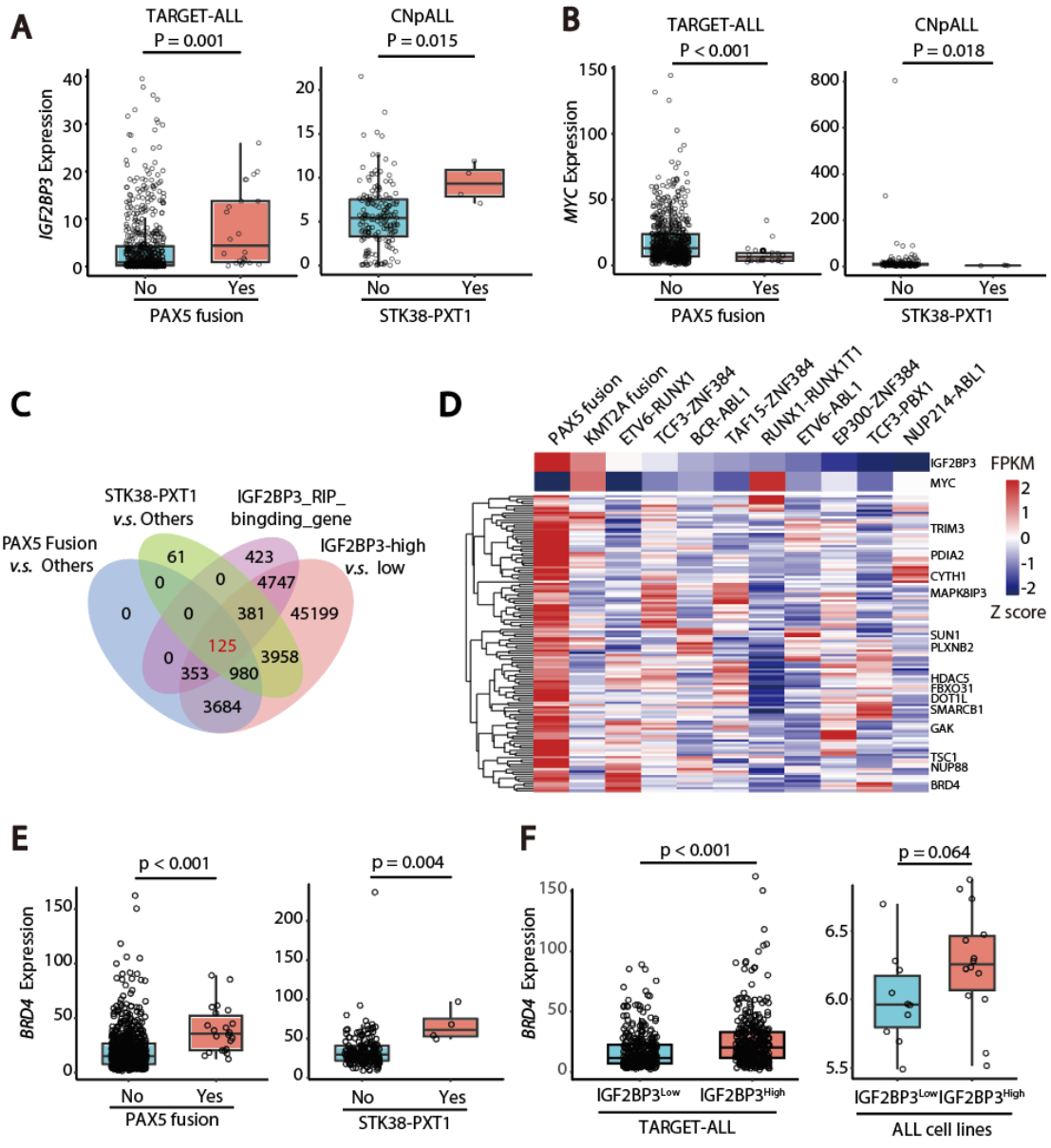

Figure S6. The potential downstream of IGF2BP3 as well as the mechanism of IGF2BP3

upregulation in the PAX5 fusion or STK38-PXT1 positive ALL. (**A**) *IGF2BP3* mRNA expression in cases with or without PAX5 fusions (TARGET-ALL, left) and STK38-PXT1 (CNpALL, right). (**B**) *MYC* mRNA expression in the same comparisons as in (A) for TARGET-ALL (left) and CNpALL (right). (**C**) Venn diagram showing overlap among DEGs in PAX5-fusion versus other ALL, STK38-PXT1 versus other ALL, IGF2BP3 RIP-seq binding targets, and genes higher in IGF2BP3-high versus IGF2BP3-low samples. (**D**) Heat map of *IGF2BP3*, *MYC*, and 125 overlaid genes in (C). (**E**) *BRD4* expression in PAX5-fusion (TARGET-ALL, left) and STK38-PXT1 samples (CNpALL, right). (**F**) *BRD4* expression stratified by IGF2BP3 level in TARGET-ALL (left) and in ALL cell lines (right). (A, B, E, F) The significance analysis was conducted by two-tailed unpaired Student's t-test.

Figure S7

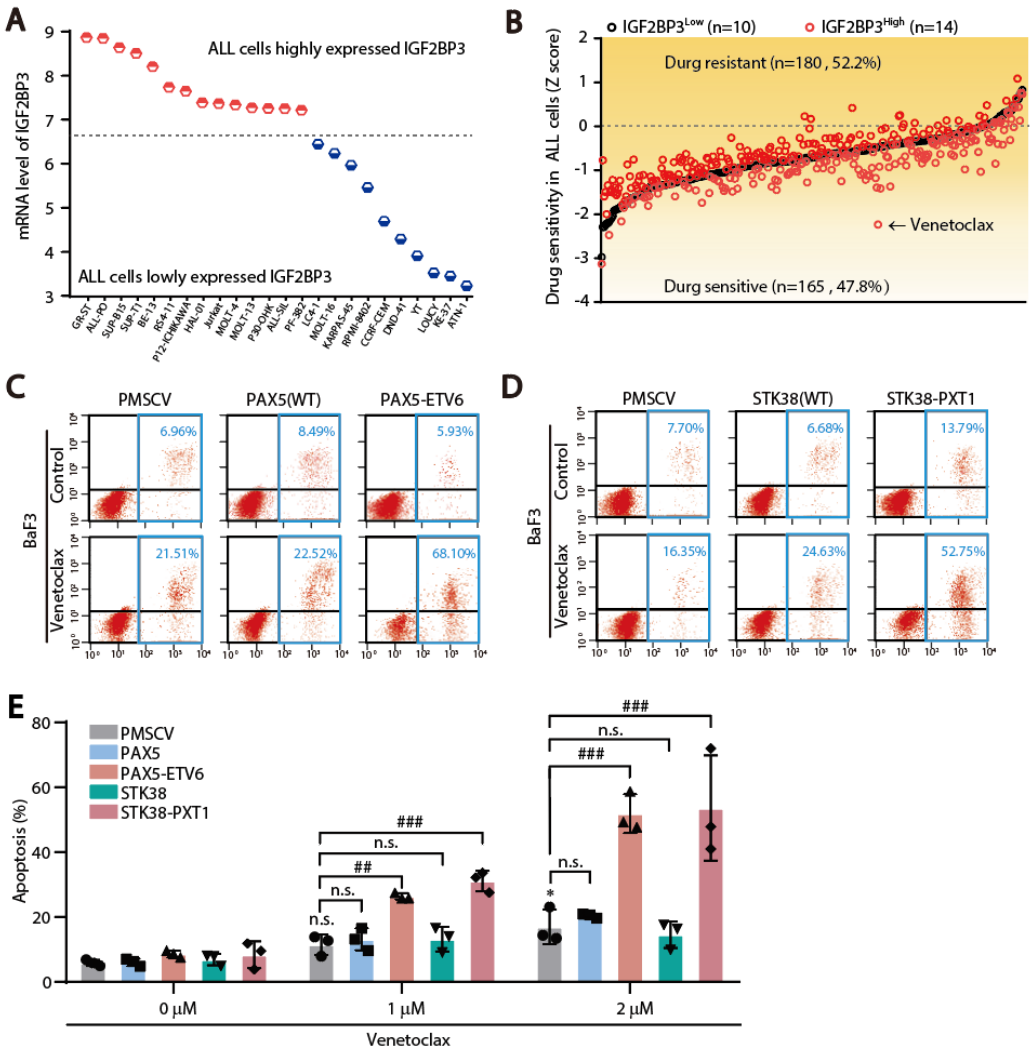

Figure S7. The effect of venetoclax on the cells with PAX5-ETV6 or STK38-PXT1. (**A**) Expression levels of IGF2BP3 in 24 ALL cell lines in GDSC database. According to the expression level of IGF2BP3, the 24 ALL cell lines were divided into 14 cell lines with high expression (red) and 10 cell lines with low expression (blue). (**B**) Z score, the mean sensitivity score, of 24 ALL cell lines mentioned above to 345 anti-tumor compounds. IGF2BP3 Low: Z score of 10 cell lines with low levels of IGF2BP3 expression, marked in black; IGF2BP3 High: Z score of the 14 cell lines with high levels of IGF2BP3 expression, marked in red. (**C**) Representative flow-cytometry plots showing venetoclax-induced apoptosis in Ba/F3 cells overexpressing vector-PMSCV, PAX5 (WT), or PAX5-ETV6. (**D**) Representative flow-cytometry plots showing venetoclax-induced apoptosis in Ba/F3 cells overexpressing vector-PMSCV, STK38 (WT), or STK38-PXT1. (C-D) Apoptosis of cells induced by 2μM venetoclax was investigated by flow cytometry with Annexin V/PI double staining. (**E**) Quantification of venetoclax-induced apoptosis in BaF3 cells overexpressing vector-PMSCV, PAX5(WT), PAX5-ETV6, STK38(WT) and STK38-PXT1. (E) Data are represented as mean ± SD (n=3). The significance analysis was conducted by one-way ANOVA analysis. n.s., P>0.05; *, P<0.05 vs. PMSCV. n.s., P>0.05; ##, P<0.01; ###, P<0.001 vs. indicated.

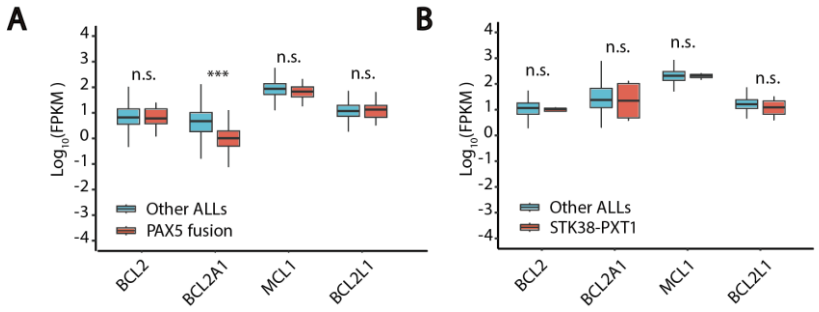

Figure S8. The expression level of anti-apoptotic family proteins in ALL with PAX5 fusion or STK38-PXT1. (**A**) Log_{10}(FPKM) of BCL2, BCL2A1, MCL1, and BCL2L1 in PAX5 fusion versus other ALLs (TARGET-ALL). (**B**) Log_{10}(FPKM) of the same genes in STK38-PXT1 versus other ALLs (CNpALL). (A, B) The significance analysis was conducted by two-tailed unpaired Student's t-test. n.s., P>0.05; ***, P<0.001.

Supplementary tables

Table S1. Specific PCR primers

Name	Specific PCR primers
GAPDH-F	GTCATCCATGACAACTTTGG
GAPDH-R	GAGCTTGACAAAGTGGTCGT
PAX5-F	GAAAAATTATCCGACTCCTC
PAX5-R	TGTGACTGGAAGCTGGGACTG
STK38-F	AGCACATGCTCGGAAGGAAA
STK38-R	GAACAAGCCGTACCTCACCA
Igf2bp3-F	CAAAGGGGTTGGGGAGGAAG
Igf2bp3-R	ATGGAGCCGGTGGATTTTGT

Table S2. The fusions with mRNA upregulation of partner gene.

Fusion.name	**Left partner gene**		**Right partner gene**	
	log_2FC	log_{10}(P_value)	log_2FC	log_{10}(P_value)
AL713998.3--AL713998.1	6.222048	2.134122243	5.791141	1.841809223
PDCD6IPP1--AC138649.5	4.86912	1.764061415	5.166115	3.634786228
PHACTR3--RBM38	4.701417	6.272734997	1.971395	5.018697322
AC139491.6--AC139491.8	4.599559	14.22716379	5.764199	9.670982801
SIK1--SERINC2	3.840083	1.71404285	2.458446	2.192216512
AC006427.2--TAPT1-AS1	3.643966	1.761458682	1.826769	1.438534951
AC110023.1--AC091078.1	3.058589	3.282287334	3.008313	2.900328077
SLC7A5--ZFPM1	2.614066	1.766959358	2.759086	1.060941258
PIM3--PLXNB2	2.518564	1.775492059	2.187941	1.686920832
RNU6-3P--SNORD13	2.454678	2.076627979	1.809349	1.411251677
GLT1D1--SLC15A4	2.397478	1.643675477	1.851806	1.725990649
LINC00621--SLC25A13	2.356188	1.348566296	2.304524	1.060942188
RNU6-9--SNORA20	2.315168	11.08128863	1.094784	4.302725212
AC008740.1--CRYM-AS1	2.214831	5.458771323	2.137733	5.581563853
CTSD--LSP1	2.167376	1.659978638	1.287203	1.363803275
RNU6-2--SNORD13	2.113436	13.69015362	1.801866	13.98454563
PAX5--ETV6	2.105401	3.298874131	1.604696	3.3960304
PAX5--NOL4L	2.082179	2.113837942	2.401667	2.462575011
SLC7A5--CBFA2T3	2.081732	2.777109361	1.117829	0.68931774
MKNK2--MOB3A	1.968826	6.092565238	1.992339	6.8416633
SIK1--KLF2	1.946382	1.503318294	1.263268	1.427811573

FLT1--CDX2	1.910141	1.909698103	9.928784	2.518161477
RNU6-9--SNORD13	1.850025	1.83783521	1.683141	1.483806425
RNU6-33P--Z93241.1	1.840877	9.636695131	1.391302	4.951582748
PAX5--AUTS2	1.801358	1.427010118	2.676011	1.796913581
RNU6-4P--TMEM107	1.798287	2.995319533	1.090378	1.397981433
YPEL5--GNAS	1.793707	4.039126132	1.092312	3.593744883
RNU6-33P--SNORD13	1.758092	2.660786228	1.916942	1.854911133
MKNK2--METRNL	1.661278	2.485593428	1.269334	2.428944366
PAX5--CBFA2T3	1.617686	1.647705178	1.240506	1.806007696
ZEB1--GNAS	1.610407	1.643675477	1.694615	1.06067047
NUP214--ABL1	1.550979	1.778422723	1.551588	1.787516336
SLC66A2--CTDP1	1.524007	2.790264913	1.430831	1.369098227
ZCCHC7--PAX5	1.416107	1.480614788	1.397932	1.571258862
MEF2D--HNRNPUL1	1.404458	1.512580764	1.072729	1.560288161
AL365295.1--AL356020.1	1.383408	1.995268624	1.403986	5.394051996
ETV6--ARNT	1.337475	1.556284643	3.509374	1.835795692
PLEKHO2--SLC51B	1.205654	1.349005212	3.656317	2.010477727
PABPC1--EIF1B	1.200483	2.43930395	1.960306	2.861206281
PAX5--ZCCHC7	1.191649	1.894716082	1.148316	1.951070679
STK38--PXT1	1.189507	3.041253327	4.363556	3.152875952
NOL4L--RBM38	1.172027	1.44238654	1.638697	1.438534823
LPCAT1--CLPTM1L	1.132157	1.796601183	1.286005	2.461716995
CTDP1--NFATC1	1.129225	2.216063689	2.823167	1.074809362
TPM4--PTMA	1.098715	1.362558488	1.292914	1.662029018
MOB3A--GNA15	1.087105	1.958851932	1.331997	2.711614965
BSG--RNF126	1.055961	1.340157582	1.369012	1.754198856
MKNK2--REXO1	1.02069	1.319644545	1.009528	1.659978638
DUX4L4--IGH-@-ext	10.26654	60.38100704	-0.691958	0.132456367
DUX4L4--IGH@-ext	6.810196	15.18101248	-1.507835	0.391179905
TLX1NB--TRDC	6.153203	1.331675517	-0.730636	0.399603991
AC093642.5--RPL23AP60	5.726451	1.735665329	-13.09306	0.019201268
TLX1NB--RPP30	5.575933	2.293823619	0.741371	1.450105111
NKX2-1--TRAJ42	5.129953	1.335199331	0.042343	0.487678455
SIK1--GNAS	4.863286	1.793284543	-0.10745	0.145274497
DUX4--IGH@-ext	4.649656	9.02165989	-1.507835	0.391179905
SFTA3--TRDC	4.04183	1.490716004	0.075894	0.490071166
SIK1--PTMA	3.278034	3.276562988	0.197299	0.319857808
TRDV2--TRAC	3.221798	15.6876546	0.751805	3.583063541
NKD2--SLC12A7	3.198069	2.866334479	0.500602	1.185859146
SEMA6A--FEM1C	3.002357	1.670306271	0.812881	4.714339513
AC007952.4--SNORD3H	2.884153	1.041955939	8.674227	3.530850856
SIK1--ACTB	2.668294	2.180045659	-0.053547	0.117140961
BCL9--MEF2D	2.641028	1.818463484	0.175216	0.300370928
DUX4--IGH-@-ext	2.550988	8.754919041	-1.183849	0.13403449

SYTL3--EZR	2.378346	1.485022989	0.410461	0.531947913
PIM3--CRELD2	2.284602	1.653772609	0.716197	0.785135412
RNU6-3P--RPL23	2.275656	1.700006448	0.977521	1.295896892
RNU6-3P--EIF4A2	2.224215	3.825448441	-0.132799	0.192578829
RNU6-9--CSKMT	2.216114	26.93004357	0.728535	8.13863336
RNU6-4P--SNORA20	2.205429	21.03201052	0.601532	7.609866472
BCL2L11--PTMA	2.197166	2.900815977	0.235907	0.512538447
RNU6-3P--SNHG12	2.169115	4.297595314	0.61965	1.853470271
ZNF384--TCF3	2.164294	1.725990649	-0.831292	0.423190576
RNU6-9--SCARNA11	2.125562	4.950229205	0.34445	1.978111169
MKNK2--DAZAP1	2.105134	2.155955332	-0.501932	0.437985664
MAFF--CSNK1E	2.07668	10.81198971	0.518081	4.205758205
RNU6-33P--RPSA	2.075424	8.353135154	0.683799	2.409292758
RNU6-36P--EIF4A2	2.071509	4.349438344	-0.065109	0.00600977
PIK3R5--UBB	2.070434	1.627452128	-0.694601	0.966242707
PAX5--BCOR	2.066366	1.52840224	0.534798	0.817279853
RNU6-3P--NCL	2.060368	13.44153846	-0.046821	0.283150874
GNA11--SGTA	2.040955	1.742693797	0.90639	1.082670945
FBRSL1--NOC4L	2.024921	3.715905095	0.289741	0.822837255
GNA11--CSNK1G2	1.995971	1.692824648	0.136743	0.32723613
RNU6-4P--SNORA14B	1.957311	7.911963037	0.643799	3.174087354
RNU6-1--RPL23	1.954321	1.596551321	0.810292	0.90480322
PIM3--BRD1	1.925519	7.011071538	0.772686	1.493731766
MAFK--PTMA	1.907675	1.516118085	0.043648	0.044135327
CXCR4--RBM38	1.898152	1.069427035	1.411131	1.321628025
MKNK2--DOT1L	1.89701	2.59074734	0.775478	1.521938439
PFKFB3--RBM17	1.88239	1.438973848	0.372886	0.916480242
NKD2--CLPTM1L	1.836044	1.537549677	0.531266	0.785859446
YPEL5--PTMA	1.810482	8.131180234	0.282185	1.314909724
FGFRL1--CTBP1	1.796572	3.376841466	-0.236854	0.029363192
GNA12--RNPC3	1.796084	1.611308529	0.051339	0.072067097
RORA--B2M	1.787104	1.516118085	0.098801	0.171665964
MAP2K3--TMEM11	1.768672	1.643675477	0.026234	0.060716321
NADK--SSU72	1.750879	1.838607474	0.11106	0.246761111
SEMA6A--NR3C1	1.748182	1.363803275	0.35229	0.343584093
AC078983.1--CAND1	1.723392	2.060855526	0.242447	0.400079092
TAL1--TRDC	1.701255	1.306894737	0.663506	1.038796387
CDKN1A--EEF1A1P5	1.676123	2.115963778	0.420951	0.962348828
SENP3-EIF4A1--GNAS	1.653588	1.725995497	0.35975	0.867929142
MKNK2--CSNK1G2	1.632167	1.490601217	0.01594	0.139265334
FOCAD--LINC01239	1.589218	1.068601532	6.106922	2.185785454
SLC16A3--RNF166	1.574675	1.122860951	2.080496	1.759477123
TXLNG--AP1S2	1.535681	1.759477123	0.884202	1.219346502
AC010332.1--ZNF880	1.513516	0.859356959	1.554774	1.576353064

MAFK--SUN1	1.509876	1.354209525	0.89497	1.014452101
ABL1--BCR	1.493564	2.372857499	0.148172	0.29106765
CDKN1A--GNAS	1.438914	1.423782123	-0.004348	0.101497292
KLF10--YWHAZ	1.391784	13.47151315	0.261255	2.482086545
KLF10--AZIN1	1.383321	10.38847331	0.427835	2.134252348
PIM3--PTMA	1.342965	1.692824648	-0.252799	0.220309735
GNA15--MOB3A	1.322221	1.298261364	1.923496	1.736291832
AC131097.3--THAP4	1.320508	3.321934242	0.583736	1.902714941
ITGB2--SUMO3	1.316731	4.744958218	0.200213	0.326256051
AC244502.1--TLX1NB	1.30984	0.751531255	6.242535	1.337754601
ARHGEF7--ING1	1.29711	2.290225974	-0.111987	0.001763831
LSP1--SF1	1.287203	1.363803275	0.132153	0.272143969
SH3TC1--IGH@-ext	1.282154	1.378679924	-0.82903	0.107565907
ARHGAP12--AC012494.1	1.271837	0.959673438	8.168267	2.135541207
MOB3A--IGH@-ext	1.268871	2.457185795	-0.96385	0.0234908
SCAF4--MYH9	1.189933	1.595244616	0.586191	1.261862923
B3GNT5--KLHL24	1.186879	8.1670402	0.050257	0.190959229
CXCR4--PTMA	1.167698	7.705823183	0.795451	9.376443917
SENP3-EIF4A1--METRNL	1.158849	0.978875896	1.156319	1.45424452
FLT1--HMGB1	1.158563	2.175162409	0.185988	0.331303519
BACH2--SYNCRIP	1.146014	2.812439616	0.385664	2.061691199
SLC7A5--BANP	1.136214	5.158198541	0.839304	4.936070986
SCAF4--SON	1.105797	1.516118085	0.67122	1.1913914
BACH2--PNRC1	1.09307	1.455203223	0.500557	1.490439282
YPEL5--BCL11A	1.080265	2.557340429	0.855468	1.58134776
YPEL5--YWHAZ	1.05862	1.393635234	0.301544	0.571357393
PRDM10--APLP2	1.047056	1.393635234	-0.026054	0.234790927
ZNF384--EP300	1.044715	3.02929014	0.093761	0.516636176
LATS2--ZMYM2	1.023834	6.812329484	0.246897	2.4052188
YWHAZ--ZNF706	1.018671	1.775492059	0.315192	1.772815414
YPEL5--FOSL2	1.014619	1.26678974	1.166204	3.328234925
SH3TC1--TBC1D14	1.004686	2.038956335	0.601059	0.839350711
RUNX1--LHFPL3-AS1	-0.854597	0.201465225	10.39868	2.498071182
MLLT10--AC097462.3	0.465618	0.551948923	10.1463	1.514435222
ITPR1--RIT2	0.505513	0.506957152	9.824007	1.984285788
PGS1--GIP	0.384528	0.68931774	9.670081	1.859531426
CCDC26--AC103718.1	0.790115	0.986725065	8.88815	1.838040324
TCF3--HLF	0.812444	1.374308526	8.198867	3.235485537
TCF3--PBX1	0.895484	4.197595268	7.969384	8.093606845
PRKCB--CACNG3	-0.521821	0.172416285	7.903027	1.635523522
RUNX1--RUNX1T1	-0.047595	0.130771164	7.633872	2.575342775
ZCCHC7--AC114757.1	0.830649	0.587609992	7.318608	1.39515141
CRBN--GABRB2	-0.61754	0.628745335	7.244197	2.596598089

EWSR1--FEV	-1.744699	1.032657383	7.067241	1.391735204
RUNX1--BCL2L14	0.006252	0.450743807	6.957345	1.933064772
FDFT1--DEFB135	0.216829	0.284619685	6.517531	10.03804189
OAZ1--PQLC1	0.903537	1.042468011	6.425012	13.06550717
MAD1L1--ELFN1	0.892929	0.334849272	6.394255	1.835740032
RUNX1--MMP16	0.335835	0.705906845	6.367398	1.88692166
TPGS2--CCDC178	-0.414049	0.241900789	6.324548	1.46081299
USP9Y--XGY1	-5.705099	0.166676487	6.150875	1.572571222
B2M--AC107398.3	0.185868	0.392192913	5.699795	1.810781928
DIAPH1--JAKMIP2-AS1	-0.042938	0.052269846	5.456419	2.027119725
ETV6--BCL2L14	-1.43195	1.043171618	5.260303	3.372552419
PSMD2--ECE2	0.043883	0.100477399	5.178203	1.413019686
KMT2A--CT45A1	-1.262666	0.657910572	5.121956	2.372128999
AC131097.3--AC093642.5	0.422351	0.237317085	5.079359	6.810836714
CPSF6--SPATA48	-0.552948	0.627738925	5.05181	1.839911491
CD74--CAMK2A	-0.904951	3.042408181	4.672377	8.953540282
IGH-@-ext--CRLF2	0.242889	0.153471236	4.632812	3.061106047
GPSM2--SPATA42	-0.182091	0.028821434	4.397726	1.388255956
SLC12A7--IRX2	0.940984	0.688516243	4.271735	5.872147541
CD81--DUSP8	-0.805118	1.025776127	4.008108	4.314581011
IGH@-ext--DUX4L4	-1.487923	0.036312868	3.760177	5.221065813
P2RY8--CRLF2	-0.792397	0.955813139	3.687682	3.10480948
B2M--SKI	0.737025	0.901717781	3.544577	1.771223212
EIF4A1--KLF2	-0.364888	0.259420026	3.528952	2.479069303
TTYH3--PDGFA	-0.226552	0.405446555	3.372324	2.483201805
EBF1--PDGFRB	0.655933	0.514164573	3.353728	1.703618297
OAZ1--KLF2	0.200338	0.283470093	3.337182	6.060896601
CD74--ARSI	-0.484012	1.76234915	3.268155	11.07016078
SLC12A7--NKD2	0.36261	0.434416194	3.238995	2.390267549
MAFK--PDGFA	0.638339	2.298743939	3.160024	4.845746714
IGH@-ext--DUX4	-1.487923	0.036312868	3.108713	3.373665264
IGH-@-ext--DUX4	-2.405588	0.2214723	3.053589	3.304396159
ARID4B--GNG4	-0.38465	0.204317157	2.979813	1.703621533
MEF2D--BCL9	0.325981	0.561573664	2.95063	2.541422904
PAX5--VPS9D1-AS1	-1.601833	0.052269849	2.873202	1.796913581
OAZ1--TMPRSS9	0.033241	0.138834114	2.827957	1.81031046
LAPTM5--SERINC2	0.394437	0.855979871	2.774279	1.776340686
MAD1L1--PDGFA	0.822349	0.928807039	2.75312	1.643677006
PIM3--SIK1	0.630783	1.122511277	2.656698	2.176856738
CBFA2T3--ZFPM1	0.836132	1.038773643	2.616418	1.775492168
ANKRD11--SLC7A5	0.989449	1.38136395	2.614066	1.766959358
B2M--RBM38	0.317001	0.614658265	2.608318	1.775492032
OAZ1--SERINC2	-0.451243	0.611345802	2.466227	2.689110402
SH3TC1--WFS1	0.17695	0.503412567	2.165493	2.083520727

TCF3--ZNF384	-0.202669	0.178297246	2.164294	1.725990649
OAZ1--MKNK2	-0.428086	1.093063016	2.162514	4.991195543
U3--KCTD1	-0.085534	0.265598498	2.154447	7.164936042
GSE1--SLC7A5	0.438568	0.633048726	2.150025	1.982616486
PPP6R2--SCO2	-0.269515	0.420542564	2.08562	1.725990649
BCOR--PAX5	0.534798	0.817279853	2.066366	1.52840224
JARID2--PTP4A1	0.337347	0.751806892	2.025401	1.62745969
PLXNB2--SCO2	-0.068101	0.234708434	2.016351	2.192216512
OAZ1--REXO1	-0.249692	0.271209703	1.869666	1.827119238
ST3GAL1--NDRG1	0.86738	8.629284776	1.852136	18.82898612
TRABD--SCO2	-0.962742	0.797359207	1.820837	1.563355593
YWHAZ--KLF10	0.292077	1.358612977	1.778159	9.860938405
CYTH1--USP36	0.7792	10.69859267	1.769663	19.18328324
SBF1--SCO2	-0.230157	0.098582041	1.744357	1.924078524
ETV6--NCOA2	0.823411	0.681226398	1.714163	1.637320947
LMNB2--MKNK2	0.57558	0.718422002	1.669642	1.676361675
KLHDC4--SLC7A5	-1.14745	1.108990897	1.663555	1.649652019
GPSM1--RALGDS	0.080206	0.392192918	1.647572	1.6046623
OAZ1--KLF16	-0.320881	1.271592476	1.611146	4.480461585
LAPTM5--TSC22D3	0.746147	1.643675477	1.583448	1.45424452
HNRNPK--DAPK1	0.255355	0.864407446	1.534868	2.303911415
EGFL7--AGPAT2	0.205877	0.42406424	1.534234	2.711617643
CBFA2T3--SLC7A5	0.493413	1.511061806	1.528605	4.426929751
GPSM1--NOTCH1	0.978447	0.964346262	1.469931	1.595244616
TTYH3--LFNG	0.912733	1.35672781	1.412477	2.833217006
PFKP--KLF6	-0.078042	0.234311399	1.40846	3.902035016
SLC12A7--CLPTM1L	0.044563	0.145312828	1.392098	2.023400813
RGPD5--BCL2L11	0.804401	1.466626905	1.35564	1.82496488
MBP--ZNF516	0.237228	0.785696582	1.34967	4.084063992
OAZ1--TCF3	0.694768	0.017489021	1.346664	2.132930029
ZC3H7A--SNN	0.826674	1.500530924	1.344521	1.393635234
YWHAE--CRK	0.861654	1.588455014	1.34292	1.60872672
BCR--ABL1	-0.201064	0.12961818	1.338937	4.923060986
HMGN2--STMN1	0.859339	1.508820818	1.31679	1.814217768
DDX3X--MLLT10	-0.946216	0.861774044	1.311994	2.332636373
OR51S1--TP53I11	-2.63103	0.689008836	1.311833	11.76059439
MTAP--CDKN2B-AS1	-0.447408	0.281106494	1.301153	2.363139981
BANP--SLC7A5	0.794949	2.262069411	1.293492	4.458361579
FBRSL1--RBM38	0.020104	0.420542564	1.239836	1.627452128
AGPAT3--SUMO3	0.129924	0.242129704	1.238352	1.70936762
YAF2--RYBP	0.359041	3.637435302	1.225131	8.531883765
G3BP2--CNOT6L	0.708022	1.563355593	1.21743	1.45424452
MAD1L1--MAFK	0.471469	1.620410637	1.209478	2.208348153
OAZ1--SGTA	0.627124	0.020014493	1.179691	2.234393284

CXCR4--GNAS	0.893958	1.510749519	1.169315	2.616440091
GALNS--RNF166	0.850203	0.448030957	1.164768	2.154901604
GRAMD4--CERK	0.446789	0.732561518	1.157083	3.101243823
HNRNPA1P49--HNRNPA1	0.538255	0.633003909	1.141056	1.766959358
TTYH3--METRNL	0.163888	0.045120532	1.135452	3.477334011
CXCR4--KLF11	0.159951	0.356424241	1.130711	1.306195395
B2M--GNAS	0.386147	1.811379658	1.127635	7.983650443
CPSF6--CSNK1D	0.141351	0.303222124	1.120189	1.363803275
NUP98--RAP1GDS1	-0.349163	0.310382214	1.111837	1.385140115
OAZ1--METRNL	0.048558	0.249315588	1.107374	3.661834016
WDR6--RBM38	-0.438711	0.676263821	1.061754	1.866881551
PPP6R2--SBF1	-0.245096	0.7227021	1.044262	2.901953674
SBNO2--TMEM259	0.9267	1.095989907	1.022378	1.692824648
TTYH3--RBM38	0.092062	0.099316976	1.021337	2.290225974
TET3--AC073046.1	0.354851	0.639527095	1.006484	1.719076732
TPM4--PTMAP5	0.557796	1.060920921	1.006114	1.455705994

Table S3. The prediction of m6A modification sites in PAX5-ETV6 fusion

Position	Partner	Sequence	Score (combined)
43	PAX5	CAGCA GGACA GGACA	0.583
48	PAX5	GGACA GGACA UGGAG	0.568
614	ETV6	AAAGA GGACU UUCGC	0.590
843	ETV6	CCAUU GAACU GUUGC	0.589
1322	ETV6	AUAGC AGACU GUAGA	0.561
1437	ETV6	CCAAC GGACU GGCUC	0.599

Table S4. The prediction of m6A modification sites in STK38-PXT1 fusion

Position	Partner	Sequence	Score (combined)
545	STK38	AAAAA AGACA CUCUG	0.564
565	STK38	AGAGG AGACU CAGUU	0.567
602	STK38	GCCAU AGACU CUAUU	0.651
662	STK38	CUUUU GGACA GCAAG	0.607
681	STK38	AUGUG AAACU UUCUG	0.582
689	STK38	CUUUC UGACU UUGGU	0.621

708	STK38	GCACA GGACU GAAAA	0.766
727	STK38	ACAUA GGACA GAAUU	0.667